BASKENT UNIVERSITY
INSTITUTE OF SCIENCE AND ENGINEERING
DEPARTMENT OF ELECTRICAL AND ELECTRONICS ENGINEERING
MASTER OF SCIENCE IN ELECTRICAL AND ELECTRONICS ENGINEERING

BLIND IMAGE DEBLURRING OF LINEAR MOTION WITH POINT SPREAD FUNCTION ESTIMATION IN FREQUENCY DOMAIN

BY

BURÇİN DAĞISTAN

MASTER OF SCIENCE THESIS

ANKARA – 2024

BASKENT UNIVERSITY
INSTITUTE OF SCIENCE AND ENGINEERING
DEPARTMENT OF ELECTRICAL AND ELECTRONICS ENGINEERING
MASTER OF SCIENCE IN ELECTRICAL AND ELECTRONICS ENGINEERING

BLIND IMAGE DEBLURRING OF LINEAR MOTION WITH POINT SPREAD FUNCTION ESTIMATION IN FREQUENCY DOMAIN

BY

BURÇİN DAĞISTAN

MASTER OF SCIENCE THESIS

ADVISOR

DR. DENİZ KARAÇOR

ANKARA – 2024

BAŞKENT UNIVERSITY
INSTITUTE OF SCIENCE AND ENGINEERING

This study, which was prepared by BURÇIN DAĞISTAN for the program of ELECTRICAL AND ELECTRONICS ENGINEERING, has been approved in partial fulfilment of the requirements for the degree of MASTER OF SCIENCE in ELECTRICAL AND ELECTRONICS ENGINEERING Department by the following committee.

Date of Thesis Defence: 19 / 08 / 2024

Thesis Title: Blind Image Deblurring of Linear Motion with Point Spread Function Estimation in Frequency Domain

Examining Committee Members	**Signature**
Dr. Deniz KARAÇOR, Başkent University	……..
Assoc. Dr. Selda GÜNEY, Başkent University	……..
Dr. Aykut KALAYCIOĞLU, Ankara University	……..

APPROVAL

Prof. Dr. Dilek ÇÖKELİLER SERDAROĞLU
Director, Institute of Science and Engineering
Date: … / … / ……..

BAŞKENT ÜNİVERSİTESİ
FEN BİLİMLER ENSTİTÜSÜ
YÜKSEK LİSANS / DOKTORA TEZ ÇALIŞMASI ORİJİNALLİK RAPORU

Tarih: 18/08/ 2024

Öğrencinin Adı, Soyadı: BURÇİN DAĞISTAN
Öğrencinin Numarası: 22110046
Anabilim Dalı: Elektrik-Elektronik Mühendisliği Anabilim Dalı
Programı: Elektrik Elektronik Mühendisliği Tezli Yüksek Lisans Programı
Danışmanın Unvanı/Adı, Soyadı: Dr. Deniz KARAÇOR
Tez Başlığı: Blind Image Deblurring of Linear Motion with Point Spread Function Estimation in Frequency Domain

Yukarıda başlığı belirtilen Yüksek Lisans/Doktora tez çalışmamın; Giriş, Ana Bölümler ve Sonuç Bölümünden oluşan, toplam 72 sayfalık kısmına ilişkin, 18/ 08/ 2024 tarihinde şahsım/tez danışmanım tarafından TURNITIN adlı intihal tespit programından aşağıda belirtilen filtrelemeler uygulanarak alınmış olan orijinallik raporuna göre, tezimin benzerlik oranı %8'dir. Uygulanan filtrelemeler:

1. Kaynakça hariç
2. Alıntılar hariç
3. Beş (5) kelimeden daha az örtüşme içeren metin kısımları hariç

"Başkent Üniversitesi Enstitüleri Tez Çalışması Orijinallik Raporu Alınması ve Kullanılması Usul ve Esaslarını" inceledim ve bu uygulama esaslarında belirtilen azami benzerlik oranlarına tez çalışmamın herhangi bir intihal içermediğini; aksinin tespit edileceği muhtemel durumda doğabilecek her türlü hukuki sorumluluğu kabul ettiğimi ve yukarıda vermiş olduğum bilgilerin doğru olduğunu beyan ederim.

Öğrenci İmzası:…….…

ONAY
Öğrenci Danışmanı
Dr. Deniz KARAÇOR
Tarih: … / … / 2024

To my beloved son Mete...

ACKNOWLEDGMENTS

I would like to express my deepest gratitude to my advisor, Dr. Deniz KARAÇOR, for unwavering support, guidance, and invaluable insights throughout the course of this research. Their expertise and dedication have been instrumental in shaping the direction and quality of this thesis.

I am also deeply grateful to the faculty and staff of the Department of Electrical and Electronics Engineering at Başkent University for providing a conducive environment for research and learning. Special thanks to Prof. Dr. Sedat NAZLIBİLEK for constructive feedback and encouragement.

I extend my heartfelt thanks to my colleagues and friends, especially Mr. Mehmet Fatih Çelik, for support, collaboration, and the many stimulating discussions that have enriched my understanding of the subject.

I am also thankful to the developers and contributors of the REDS dataset and OpenCV library, whose work has been crucial for the practical implementation of this research.

Last but not least, I owe my deepest appreciation to my family, my father Atalay ÇALIKOĞLU, my mother Emine ÇALIKOĞLU, my son Mete DAĞISTAN for their unwavering love, patience, and support. Their belief in me has been a constant source of motivation.

Thank you all for your contributions, encouragement, and support throughout this journey.

ABSTRACT

Burçin DAĞISTAN

BLIND IMAGE DEBLURRING OF LINEAR MOTION WITH POINT SPREAD FUNCTION ESTIMATION IN FREQUENCY DOMAIN

Institute of Science and Engineering

Department of Electrical and Electronics Engineering

2024

This thesis provides an in-depth examination of the issue of blind image deblurring, with a particular emphasis on linear, uniform motion blur. The primary aim of this research is to develop a fast and easy to apply methodology for restoring blurred images through precise estimation of the Point Spread Function from frequency domain and the application of Wiener deconvolution techniques.

The proposed method entails a systematic process for estimating the Point Spread Function in the frequency domain, which is subsequently utilized in Wiener deconvolution to reconstruct the original, unblurred image. Extensive experimental evaluations were conducted using Lena image and the REDS dataset, a benchmark for image restoration tasks. The performance of the proposed algorithm was assessed through both quantitative and qualitative measures. Quantitative metrics, such as Peak Signal-to-Noise Ratio (PSNR), Mena Square Error (MSE) and Structural Similarity Index (SSIM), were employed to objectively evaluate the improvements in image quality. Additionally, qualitative visual assessments further substantiated the efficacy of the proposed deblurring approach, demonstrating significant restoration of fine details and overall image sharpness.

The findings elucidate the critical role of accurate PSF estimation in the deblurring process. While the proposed method achieved promising results, it was observed that the accuracy of PSF estimation which is blur angle and blur length in this case is pivotal to the success of the deblurring algorithm. Inaccuracies in PSF estimation can lead to suboptimal restoration, introducing artifacts and diminishing image quality. Furthermore, the computational complexity associated with Wiener deconvolution presents challenges, particularly for real-time applications where processing speed is paramount.

The thesis identifies several promising avenues for future research. Enhancements in PSF estimation techniques, particularly through the incorporation of machine learning and deep

learning approaches, hold significant potential for improving accuracy and robustness. Additionally, optimizing the computational efficiency of the deblurring algorithm is essential for real-time applications, with potential strategies including parallel processing and GPU acceleration.

In conclusion, this thesis presents a significant advancement in the field of blind image deblurring, offering a rapid, less computationally complex and theoretically grounded approach to restoring images degraded by linear, uniform motion blur. The proposed methodology has demonstrated substantial improvements in image quality, paving the way for further research and development in this critical area of image processing. The findings hold considerable promise for enhancing the quality and utility of images across a wide range of applications, thereby contributing to the broader field of image restoration and analysis.

Keywords: Blind Deblurring, Linear Motion Blur, Uniform Motion Blur, Frequency Spectrum Analysis, Motion Blur Deblurring, PSF Estimation, Wiener Deconvolution

ÖZET

Burçin DAĞISTAN

BLIND IMAGE DEBLURRING OF LINEAR MOTION WITH POINT SPREAD FUNCTION ESTIMATION IN FREQUENCY DOMAIN

Başkent Üniversitesi Fen Bilimleri Enstitüsü

Elektrik-Elektronik Mühendisliği Anabilim Dalı

2024

Bu tez, kör görüntü bulanıklığını giderme sorununu, özellikle doğrusal, tek tip hareket bulanıklığına odaklanarak derinlemesine incelemektedir. Bu araştırmanın birincil amacı, bulanık görüntüleri, Nokta Yayılım Fonksiyonu'nun (PSF) doğru tahmini ve Wiener dekonvolüsyon tekniklerinin uygulanması yoluyla hızlı ve kolay uygulanabilir bir yöntem geliştirmektir.

Önerilen yöntem, frekans alanında Nokta Yayılım Fonksiyonu'nun (PSF) sistematik bir şekilde tahmin edilmesini ve ardından orijinal, bulanık olmayan görüntüyü yeniden oluşturmak için Wiener dekonvolüsyonunun kullanılmasını içermektedir. Lena görüntüsü ve görüntü iyileştirme görevleri için bir kıstas olan REDS veri kümesi kullanılarak kapsamlı deneysel değerlendirmeler yapılmıştır. Önerilen algoritmanın performansı hem nicel hem de nitel ölçütlerle değerlendirilmiştir. Görüntü kalitesindeki iyileşmeleri nesnel olarak değerlendirmek için Tepe Sinyal-Gürültü Oranı (PSNR), Ortalama Karesel Hata (MSE) ve Yapısal Benzerlik İndeksi (SSIM) gibi nicel metrikler kullanılmıştır. Ayrıca, nitel görsel değerlendirmeler, önerilen bulanıklık giderme yaklaşımının etkinliğini daha da doğrulamış, ince detayların ve genel görüntü keskinliğinin önemli ölçüde geri kazanıldığını göstermiştir. Bu araştırma, doğrusal, tek tip hareket bulanıklığının teorik anlaşılmasına önemli bir katkı sağlamaktadır. Nokta Yayılım Fonksiyonu (PSF) kavramı ve matematiksel temsili üzerine derinlemesine bir tartışma sunmaktadır. Bulgular, bulanıklık giderme sürecinde doğru PSF tahmininin kritik rolünü açıklamaktadır. Önerilen yöntem umut verici sonuçlar elde etmiş olsa da bulanıklık açısı ve bulanıklık uzunluğu gibi PSF tahmininin doğruluğunun, bulanıklık giderme algoritmasının başarısı için çok önemli olduğu gözlemlenmiştir. PSF tahminindeki hatalar, optimal olmayan iyileştirmelere yol açabilir, artefaktlar oluşturabilir ve görüntü kalitesini düşürebilir. Ayrıca, Wiener dekonvolüsyon ile ilişkili hesaplama karmaşıklığı, özellikle işlem hızının çok önemli olduğu gerçek zamanlı uygulamalarda zorluklar sunmaktadır.

Tez, gelecekteki araştırmalar için birkaç umut verici alan belirlemektedir. Özellikle makine öğrenimi ve derin öğrenme yaklaşımlarının dahil edilmesi yoluyla PSF tahmin tekniklerindeki iyileştirmeler, doğruluk ve dayanıklılığı artırma potansiyeline sahiptir. Ayrıca, bulanıklık giderme algoritmasının hesaplama verimliliğini optimize etmek, paralel işlem ve GPU hızlandırma gibi potansiyel stratejilerle gerçek zamanlı uygulamalar için gereklidir.

Sonuç olarak, bu tez, doğrusal, tek tip hareket bulanıklığı ile bozulmuş görüntüleri geri kazandırmak için hızlı, daha az hesaplama karmaşıklığına sahip ve teorik olarak sağlam bir yaklaşım sunarak kör görüntü bulanıklığını giderme alanında önemli bir ilerleme sunmaktadır. Önerilen yöntem, görüntü kalitesinde önemli iyileşmeler göstermiş, bu kritik görüntü işleme alanında daha fazla araştırma ve geliştirme için yol açmıştır. Bulgular, geniş bir uygulama yelpazesinde görüntülerin kalitesini ve kullanılabilirliğini artırma konusunda önemli bir potansiyele sahiptir ve böylece görüntü iyileştirme ve analizinin daha geniş alanına katkıda bulunmaktadır.

Anahtar Kelimeler: Kör Görüntü Bulanıklığı Giderme, Tek Tip Hareket Bulanıklığı, Frekans Spektrum Analiz, Hareket Bulanıklığı Giderme, PSF Tahmini, Wiener Dekonvolüsyonu

TABLE OF CONTENTS

Page

ACKNOWLEDGMENTS i
ABSTRACT ii
ÖZET iv
TABLE OF CONTENTS vi
LIST OF FIGURES viii
LIST OF TABLES xi
LIST OF ABBREVIATIONS xii
1. INTRODUCTION 1
1.1. Importance of Image Deblurring in Various Applications 1
1.2. Types of Blurs and Their Effects on Images 5
1.3. Traditional Deblurring Methods and Their Applications 7
1.3.1. Linear Methods 8
1.3.2. Nonlinear Methods 10
1.3.3. Frequency Domain Methods 13
1.3.4. Iterative Methods 15
1.3.5. Comparative Analysis 17
1.4. Point Spread Function Estimation 18
1.4.1. Non-Blind PSF Estimation 18
1.4.2. Blind PSF Estimation 18
1.5. REDS Dataset 19
1.6. Proposed Approach 21
2. THEORY 22
2.1. Image Formation Model 22
2.1.1. Image Acquisition Process 22
2.1.2. Convolutional Model for Image Degradation 25
2.2. Linear Motion Blur 27
2.2.1. PSF Concept and Its Role in Motion Blur 28
2.2.2. Mathematical Representation of Motion Blur Kernel 30
2.3. Frequency Domain Analysis 31
2.3.1. Fourier Transform Concept 31

2.3.2. Frequency Spectrum of Blurred Images 32
2.4. Frequency Spectrum Analysis for PSF Estimation 34
2.4.1. Properties of the Frequency Spectrum Under Motion Blur 34
2.4.2. Logarithmic Transformation 35
2.4.3. Techniques for Extracting Blur Parameters from the Spectrum 37
2.5. Wiener Deconvolution for Image Restoration 38
2.5.1. Mathematical Formulation of the Wiener Filter 38
2.5.2. Properties and advantages of Wiener Deconvolution 39
3. MOTIVATION 40
3.1. APPLICATION 40
3.1.1. Hough Transform Method to Estimate PSF: Review on Literature and an Algorithm 40
3.1.2. Radon Transform Method to Estimate PSF: Review on Literature and an Algorithm 43
3.1.3. Cepstrum Analysis Method: Review on Literature 48
3.2. PURPOSE 51
4. METHOD 52
5. EXPERIMENTAL RESULTS & DISCUSSION 54
5.1. Blur Angle Estimation 54
5.2. Blur Length Estimation 57
5.3. Wiener Deconvolution 62
5.4. Application on REDS Dataset 64
6. CONCLUSION AND FUTURE WORK 71
6.1. Conclusion 71
6.2. Future Work 72
REFERENCES 74

LIST OF FIGURES

Page

Figure 1.1.Denoising Performance of the Recommended Algorithm on Different Gaussian Noise Patterns [3] 2
Figure 1.2.Registered and Restored Images [4] 3
Figure 1.3.Deblurring results of a typical surveillance scene in an urban environment [5] 4
Figure 1.4.Image Deblurring Practices for Remote Sensing Applications [6] 4
Figure 1.5.Image Spoiled by Camera Shake and Results of Deblurring Algorithm [7] 5
Figure 1.6.Degraded and Restored Baboon Picture [8] 6
Figure 1.7.Image Reconstruction Result Taken from the Video Water Tower Distorted by Real Atmospheric Turbulence [11] 7
Figure 1.8.Aircraft Image with a Synthetic Gaussian Blur and Restored Image [14] ... 7
Figure 1.9.Sample blur(left) and sharp(right) images from REDS Dataset 21
Figure 2.1 (a) original blur image due to lens (b) deblurred image (c)original blurred image (d) (e) (f)images with deblurred using different models [62] 23
Figure 2.2. Original Lena image and linear uniform motion blurred Lena image 28
Figure 2.3.Histogram of original Lena image and histogram of linear uniform motion blurred Lena Image 28
Figure 2.4.Image without motion blur and its Fourier spectrum [28] 35
Figure 2.5.Motion blurred image with θ =45° and L=31 pixels and its Fourier spectrum [28] 35
Figure 2.6.(a) Magnitude (b) Phase (c) Imaginary part of FT image 36
Figure 2.7.Logarithmic Transform of FT image with uniform motion blur 37
Figure 3.1.Hough Transform parameters (a) x-y pixel space (b) ρ and θ parameter space [37] 41
Figure 3.2.HT for extracting motion parameters (a) cameraman image (b) motion blurred image with L=30 pixels and θ=30° (c) log spectrum (d) modified log spectrum (e) fourth bit plane of log spectrum (f) line found by HT [37] 41
Figure 3.3. HT L estimation (a) fourth bit-plane of log spectrum image (b) distracting peak points 42

Figure 3.4. HT study for spatially variant image (a) log spectrum (b) fourth bit plane [38] 42
Figure 3.5. (a) Logarithm of the power spectrum of image (white line represents direction of Radon transform) (b) Output of RT (angle θ=155°) [33] 44
Figure 3.6. Radon transform of an image in three different directions respectively β, γ, α [34] 45
Figure 3.7. RT space of image when L=16 pixels and θ =45° (x: pixels, y degrees) [35] 46
Figure 3.8. (a) Cameraman image with motion blur L=30 pixel and θ =60° (b) RT of Log spectrum of (a) [36] 46
Figure 3.9. RT for spatially variant image for L=16 pixels θ =20° and L=32 pixels and θ=60° [35] 47
Figure 3.10. (a) Motion blur free image cepstrum, (b) Motion blured image cepstrum with L=30 and θ =30° 49
Figure 3.11. Relationship between cepstrum analysis and blur length [43] 49
Figure 3.12. Cable image and its cepstrum [48] 50
Figure 5.1. (a) Sample Lenna image (b) Motion blurred Lenna image with θ =60° L=30 pixels 54
Figure 5.2. (a) LT of original Lenna image (b) LT of motion blurred image with θ =60° L=30 pixels 55
Figure 5.3. (a) LT spectrum of motion blurred image (b) Thresholded LT spectrum of motion blurred image 55
Figure 5.4. Calculations to blur angle [28] 56
Figure 5.5. PSNR of motion blurred(blue) and deblurred image(red) between θ = [-90°, +90°] when L=30 pixels 57
Figure 5.6(a) LT spectrum of motion blurred image (b) LT spectrum of rotated image with estimated angle parameter 58
Figure 5.7. (a) L=10 pixels (b) L=40 pixels 59
Figure 5.8. (a) L=10 pixels (b) L=40 pixels 59
Figure 5.9. Bit planes of rotated LT spectrum L=30 pixels 60
Figure 5.10. 4th bit plane of rotated LT spectrum L=30 pixels 60
Figure 5.11. 1D image L=30 pixels 61
Figure 5.12. PSNR of blurred(blue) and deblurred image(red) 62

Figure 5.13. (a) Blurred (b)Restored Lena Image 62
Figure 5.14 PSNR Results of Proposed Algorithm vs Number of Images 65
Figure 5.15 SSIM Results vs Number of Images 67
Figure 5.16 MSE Results vs Number of Images 69
Figure 5.17 Estimated Length vs Number of Images 70
Figure 5.18 Estimated Theta vs Number of Images 70

LIST OF TABLES

Page

Table 3.1. Algorithm - PSF Estimation with HT and Deconvolution of Blurred Image 43

Table 3.2. Algorithm – PSF Estimation with RT and Deconvolution of Blurred Image 47

Table 3.3. Algorithm – PSF Estimation with CA and Deconvolution of Blurred Image 50

Table 4.1. Algorithm Blind Image Deblurring of Linear Motion with Simple PSF Estimation in Frequency Domain and Wiener Deconvolution 52

Table 5.1. Angle estimation results on Lenna image for θ = [+90°- -90°] when L=30 pixels 56

Table 5.2 Length estimation results blur angle θ=45°, L= [10 - 40] and L= [0 - 10] 61

Table 5.3 PSNR Comparison 66

LIST OF ABBREVIATIONS

CA	Cepstrum Analysis
CCD	Charge Coupled Device
CFA	Colour Filter Array
CG	Conjugate Gradient
CMOS	Complementary Metal Oxide Semiconductor
CT	Computerized Tomography
EM	Expectation-Maximization
FFT	Fast Fourier Transform
HT	Hough Transform
IBD	Iterative Blind Deconvolution
LT	Logarithmic Transform
MRI	Magnetic Resonance Imaging
PSD	Power Spectral Density
PSF	Point Spread Function
PSNR	Peak Signal to Noise Ratio
REDS	Realistic and Diverse Scenes Dataset Realistic and Dynamic Scenes
RT	Radon Transform
SSIM	Structural Similarity Index
TV	Total Variation

1. INTRODUCTION

In this section of the thesis, an in-depth exploration of image deblurring techniques, specifically referring to linear motion blur types, will be conducted. The discourse will clarify the intricate relationship between frequency domain analysis and linear motion blur, delineating how the former can be employed to effectively mitigate the latter. Additionally, the thesis will expound upon Wiener deconvolution, detailing its application as a sophisticated filtering method for images affected by linear motion blur. This comprehensive analysis aims to augment the existing body of knowledge within the field of image processing and contribute to the advancement of deblurring methodologies.

The core of thesis is to estimate point spread function, 2D transfer function between original and blurred image, of uniform, linear, motion blurred image, which is a blur type that effects the whole image pixels same amount, from frequency domain operations, that is easy and fast according to iterative and deep learning-based methods. This method, firstly, studied on Lena image than applied to REDS dataset. Estimated point spread function than used to get deblurred image by applying Wiener deconvolution method.

1.1. Importance of Image Deblurring in Various Applications

Image deblurring is a crucial process in the field of computer vision and image processing, carrying significant implications for a wide range of applications. The primary objective of image deblurring is to reconstruct a sharp image from one that has been degraded by blur, which may result from various sources such as camera shake, motion during capture, or out-of-focus lenses. [1], [2].

Within the medical domain, the process of image deblurring is indispensable for augmenting the clarity of diagnostic imagery, thus enabling more precise diagnostic interpretations and ameliorating patient prognosis. [1]. Blur can disguise critical details in medical scans, leading to misdiagnosis or missed diagnoses. Techniques for deblurring medical images can significantly enhance the quality of diagnostic tools such as MRI, CT scans, and ultrasound images. For example, [3] provided empirical evidence that the application of sophisticated deblurring algorithms enhances the discernibility of anatomical features in ultrasound imagery, thereby contributing to improved diagnostic efficacy.

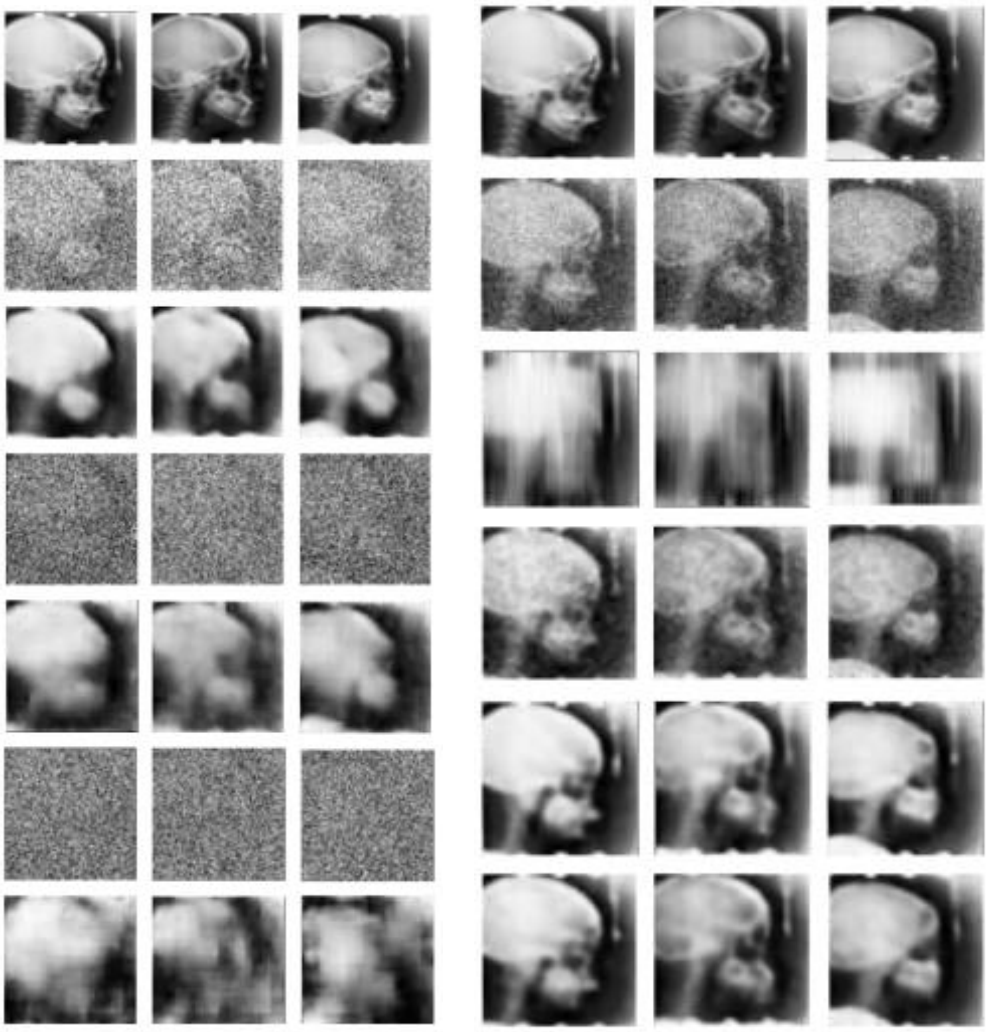

Figure 1.1. Denoising Performance of the Recommended Algorithm on Different Gaussian Noise Patterns [3]

In the field of astronomical imaging, the utility of image deblurring is significantly apparent. Telescopic captures frequently suffer from the detrimental effects of atmospheric turbulence, demonstrating as a blurring of stellar and celestial entities. The deployment of deconvolution techniques serves to mitigate these distortions, thereby facilitating astronomers with enhanced imagery that elucidates the subtler intricacies of cosmological events [4]. The research delineated in [4] underscores the capacity of image deconvolution methodologies in conjunction with deblurring algorithms, to refine the resolution of images produced.

Figure 1.2. Registered and Restored Images [4]

Surveillance systems necessitate high-resolution and meticulous imagery for precise surveillance and identification processes. Deblurring technologies play a pivotal role in preserving essential details, thus enhancing the operational efficacy of these systems [2]. In a similar vein within the photographic domain, deblurring methodologies confer advantages to both professional and amateur photographers by enabling the recovery of images that might otherwise be considered nonrecoverable due to the presence of blur [1]. The occurrence of blurred visuals from security instruments can obstruct the capacity for facial recognition, among other critical elements. The application of image deblurring techniques augments the efficiency of these systems by yielding more lucid visuals. Empirical evidence from studies indicates that the integration of deblurring algorithms into surveillance video feeds significantly raises the precision of face recognition mechanisms within security concepts [5].

Figure 1.3. Deblurring results of a typical surveillance scene in an urban environment [5]

Applications of remote sensing, containing satellite imagery and aerial photographic techniques, derive considerable advantage from the implementation of image deblurring. Such imagery is frequently applied in the realms of environmental surveillance, urban development, and crisis management. The blurring effect, attributable to the relative motion between the satellite and the Earth's surface, can diminish the feasibility of the acquired data. Deblurring methodologies contribute to the restoration of image fidelity, thereby rendering the data more subjected to analytical examination [6]. With tremendous studies it is formulated a specialized deblurring approach tailored for remote sensing imagery, peaking improved visual sharpness and superior extraction of features [6].

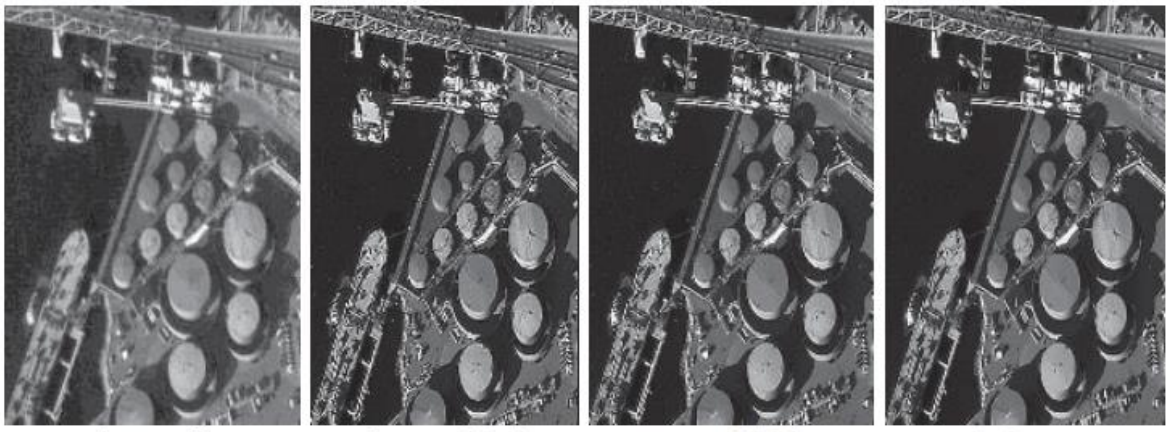

Figure 1.4. Image Deblurring Practices for Remote Sensing Applications [6]

In conclusion, the process of image deblurring is pivotal, markedly improving the quality and applicability of images within diverse fields. From medical diagnostics to celestial studies, consumer photography, security monitoring, and geospatial analysis, the deployment of proficient deblurring techniques ensures the acquisition of images with

enhanced clarity and detail, thereby supporting more thorough analysis, interpretation, and informed decision-making.

1.2. Types of Blurs and Their Effects on Images

Image blur represents a widespread form of deterioration in digital imagery, arising from a multitude of origins, each presenting unique attributes upon the affected image. Comprehending the various categories of blur and their consequential effects is essential for the formulation of powerful deblurring strategies. This discourse outlines the principal varieties of blur, encompassing motion blur, defocus blur, and atmospheric blur, alongside their implications on the measure of the image.

Motion blur happens when relative motion takes place between the camera and the scene within the duration of exposure, characterized by linear distortions or elongations in the motion's trajectory [7]. The generation of motion blur can be attributed to several factors: Camera Shake, which refers to unintended oscillations of the camera during the aperture's activation; Subject Movement, requiring the locomotion of the object being captured; and Intentional Motion, the purposeful manipulation of the camera to yield aesthetic effects. The impacts on image integrity include: Detail Loss, where minute details are obfuscated, complicating the resolution of diminutive elements; Directional Artifacts, where linear marks emerge aligned with the motion, notably evident in protracted exposure captures; and Decreased Sharpness, a pervasive diminution in sharpness, resulting in an overall smoothing of the image [7].

Figure 1.5. Image Spoiled by Camera Shake and Results of Deblurring Algorithm [7]

Defocus blur arises when the camera's optics fail to align precisely with the subject, resulting in partial or complete loss of focus across the image [8]. The causes of defocus blur can be traced to: Incorrect Focus Setting, where the lens's focal point is erroneously positioned anterior or posterior to the subject; Depth of Field, characterized by a constricted

field of focus amidst a scene presenting disparate distances from the camera. The impact on imagery includes: Blur Circles, where defocused points manifest as disc-like shapes, colloquially termed ‘bokeh’, which, while potentially visually appealing, compromise the sharpness of the image; Edge Softening, where delineations and contours within the image lose definition; and Loss of Detail**,** where granular details become veiled, challenging the discernment of features, particularly within intricately detailed zones [9].

Figure 1.6. Degraded and Restored Baboon Picture [8]

Atmospheric blur, also termed as turbulence-induced blur, arises due to heterogeneities in the atmospheric refractive index, ending up with image distortion and blurring. This phenomenon may be attributed to several factors such as heat waves, weather conditions and object distance [12]. Heat waves can induce spatial variations in the refractive index. In addition to heat waves, humidity and pressure influences the propagation of light through the atmosphere. Extended distances between the imaging instruments and the subject also amplify the probability of atmospheric interference. The indicators of atmospheric blur on imagery includes wavy distortion, variable blur and diminished clarity. Wavy distortion is a visual effect where the image appears undulated or rippled, frequently observed in long-range photography. Variable blur is a non-uniform blur intensity across the visual field, complicating consistent correction. Lastly, clarity reduction is a general degradation in image sharpness, particularly impacting fine details and high frequency elements [11].

Figure 1.7. Image Reconstruction Result Taken from the Video Water Tower Distorted by Real Atmospheric Turbulence [11]

Gaussian blur emerges as a consequence of the application of a Gaussian function, which serves to attenuate an image. This blurring modality is frequently employed within the domain of image processing, primarily to diminish noise and detail. The formation of Gaussian blur can be traced to smoothing algorithms which is caused by intentional reasons or optical system limitations which is present within the camera lens system. The impacts of Gaussian blur on photographic images are characterized by uniform blurring, noise reduction and edge blurring [13], [14].

Figure 1.8. Aircraft Image with a Synthetic Gaussian Blur and Restored Image [14]

1.3. Traditional Deblurring Methods and Their Applications

Image deblurring stands as a pivotal procedure within the domain of image processing, endeavouring to restore clarity to images that have been subject to blur due to plenty of influences, including camera instability, object movement, or focal aberrations used in various fields such as medical imaging, astronomy, and photography. It involves reversing

the blur effect that can be mathematically represented as the convolution of the true image with a Point Spread Function (PSF), often accompanied by additional noise. Conventional deblurring techniques are dependent on a robust mathematical and computational framework, encompassing methods from fundamental inverse filtering to sophisticated regularization strategies. These techniques are generally divided into four categories: linear methods, nonlinear methods, methods that operate in the frequency domain, and iterative methods [2], [13].

1.3.1. Linear methods

Linear deblurring techniques are based on the premise that there is a straightforward, proportional link between the blurred and the original image. These methods usually involve a direct reversal of the blurring effect to retrieve the initial, clear image.

1.3.1.1. Inverse filtering

Inverse filtering stands as the most fundamental approach to deblurring. With a blurred image denoted as *B* and a defined Point Spread Function (PSF) represented as *h*, the original image *I* can be estimated by reversing the convolution process within the frequency domain. In this case we ignore noise component.

$$I = \mathrm{F}^{-1}\left(\frac{\mathrm{F}(B)}{\mathrm{F}(h)}\right) \tag{1.1}$$

where F denotes the Fourier transform [13]. Although inverse filtering is a straightforward technique, it is particularly vulnerable to noise. This is because dividing by small numbers in the frequency domain can significantly increase the noise elements.

Mathematically, the degradation model can be expressed as:

$$B = I * h + n \tag{1.2}$$

where $*$ denotes convolution and *n* is additive noise [13]. The inverse filtering method seeks to recover the original image *I* by reversing the convolution of the PSF *h* from the blurred image *B* as in Eq. (1.1).

$$F\{B\} = F\{I\}.F\{H\} + F\{N\} \tag{1.3}$$

$$B(u,v) = I(u,v).H(u,v) + N(u,v) \tag{1.4}$$

$$\frac{B(u,v)}{H(u,v)} = I(u,v) + \frac{N(u,v)}{H(u,v)} \tag{1.5}$$

When the values of H(u, v) are small, it means there are high-frequency details in the image as it can be seen from equation (1.5). When we divide by these small values, any noise in those high-frequency details becomes much more pronounced. In an image, noise affects all frequencies. When we apply the inverse filter, the noise in the high-frequency parts gets amplified because we divide by small H(u, v) values. As a result, the restored image becomes noisy, particularly in the high-frequency areas, making it less visually appealing and accurate [13], [17].

Inverse filtering is often employed in scenarios where PSF is accurately determined and the presence of noise is minimal. Such circumstances are typically found in regulated settings like labs or simulations, where the blurring can be precisely replicated [17].

1.3.1.2. Wiener filtering

Wiener filtering enhances the inverse filtering technique by integrating a noise statistical model. Its objective is to reduce the average of the squared differences between the estimated image and the original image [17]. The formula for the Wiener filter in the frequency domain is presented as follows:

$$Hw(u,v) = \frac{H*(u,v)}{|H(u,v)|^2 + \frac{K}{|S(u,v)|^2}} \tag{1.6}$$

In the Wiener filtering approach, $H(u, v)$ denotes the Fourier transform of the PSF, $H*(u, v)$ represents its complex conjugate, $S(u, v)$ signifies the power spectral density of the original image, and K is a constant that quantifies the noise-to-signal ratio [17]. Wiener

filtering is designed to strike a balance between the simplicity of inverse filtering and the effectiveness of noise reduction.

Mathematically, the Wiener filter *Hw* can be expressed as:

$$Hw = \frac{H^*}{|H|^2 + \frac{N}{S}} \tag{1.7}$$

In this context, $H*$ represents the complex conjugate of the PSF within the frequency domain. Meanwhile, *N* indicates the power spectral density of the noise, and *S* refers to the power spectral density of the original signal [17].

Wiener filtering is extensively applied in fields like medical and astronomical imaging, where it's possible to know or predict the statistical characteristics of noise [18]. In medical imaging, for instance, this filtering method is instrumental in diminishing noise levels while maintaining critical diagnostic information, thereby improving the clarity of MRI or CT images [18].

On the other hand, Wiener filtering requires understanding the power spectrum of both the noise and the original signal. In real-world scenarios, accurately estimating these spectra can be a difficult task, especially when noise characteristics are unclear or the image content varies significantly [13]. Also, Wiener filtering's effectiveness relies accurately on estimating the Point Spread Function (PSF). If the PSF is not correctly determined, the filter might not effectively remove blurriness, resulting in less-than-optimal image restoration [50]. In addition to that, In Wiener filtering, we assume that the noise follows a Gaussian distribution and is added to the signal. However, if the actual noise behaves differently from this model, the filter's effectiveness may decrease importantly [17].

1.3.2. Nonlinear methods

Nonlinear deblurring approaches overcome the constraints of linear methods by incorporating nonlinearity into the deblurring equation. This enhancement allows for improved preservation of image edges and greater resilience to noise.

1.3.2.1. Total variation regularization

Total Variation regularization, a widely recognized nonlinear method, encourages the sparseness in the image's gradient, which is key to maintaining sharp edges and at the same time eliminate noise. The task of deblurring is thus approached as an optimization challenge:

$$\min_I \left(\| B - I * h \|^2 + \lambda TV(I) \right) \tag{1.8}$$

where in TV regularization approach, TV(I) represents the image's total variation, while λ serves as a parameter for regularization [19]. This method is adept at minimizing noise and safeguarding significant image features.

The TV of an image I can be defined as:

$$TV(I) = \sum i,j \sqrt{\left(I_{i+1,j} - I_{i,j}\right)^2 + \left(I_{i,j+1} - I_{i,j}\right)^2} \tag{1.9}$$

The optimization issue in question can be addressed through iterative techniques, for instance, gradient descent, or by employing more sophisticated strategies such as the split Bregman method [19].

TV regularization proves to be highly beneficial in fields like photography and surveillance, where it is essential to maintain the integrity of edge details. For photography, this technique contributes to the sharpening of images and noise reduction, which is why it's favoured in image editing applications. In the realm of surveillance, TV regularization is advantageous for augmenting the definition of images taken in conditions of dim lighting or significant movement [19].

There are also drawbacks of using TV regularization. TV minimization has a significant drawback known as the 'staircase effect.' In this effect, smooth parts of an image are reconstructed as areas with abrupt changes, creating artificial discontinuities. This issue is particularly problematic in images with gradual transitions [51]. Secondly, to use TV minimization effectively, you need to choose a regularization parameter. This parameter balances the trade-off between reducing noise and preserving the original image. However, making this choice can be difficult, as it depends on understanding both the noise level and the content of the image [52]. Since this method based on some iterative approaches,

applications can be computationally demanding and slow, especially when dealing with large images or real-time tasks. it helps maintain prominent edges, but it can also unintentionally blur fine details and textures [53].

1.3.2.2. Regularized least squares

This technique incorporates a regularization element into the least squares approach, which helps to counteract the impact of noise and the challenges of ill-posed problems. The optimization issue is thus framed as follows:

$$min_I(\| B - I * h \|^2 + \lambda \| L(I) \|^2) \tag{1.10}$$

where L represents a differential operator, such as the Laplacian, and λ is the parameter that balances the accuracy of the deblurred image with the evenness of the final result.

A frequently selected option for L is the Laplacian operator, which is characterized as follows:

$$L(I) = \nabla^2 I = \frac{\partial^2 I}{\partial x^2} + \frac{\partial^2 I}{\partial y^2} \tag{1.11}$$

The regularization term, represented by $\| L(I) \|^2$ promotes a smoother appearance in the reconstructed image, which helps to avoid the issue of the solution being too closely fitted to the noise. Also adding a regularization term usually improves how well a model predicts unseen data [54].

Regularized least squares techniques are commonly utilized in remote sensing and medical imaging due to their ability to maintain a delicate equilibrium between diminishing noise and retaining detail. Within the scope of remote sensing, these methods are instrumental in enhancing the clarity and readability of satellite imagery, which is vital for tasks such as environmental surveillance and city development planning.

Choosing the right regularization parameter (λ) is a key challenge. If λ is too big, the model becomes too simple (underfitting); if it's too small, overfitting might not be effectively controlled. Also, when we use regularization, it adds some bias to the model. While this reduces variability, if the bias becomes too strong, the model's accuracy may

suffer. This trade-off between bias and variance is important [55]. Computational complexity is another challenge.

1.3.3. Frequency domain methods

Methods operating in the frequency domain utilize the convolution theorem, which posits that convolution in the spatial domain is equivalent to multiplication in the frequency domain [21]. This principle facilitates the simplification of the image deblurring process.

1.3.3.1. Richardson-Lucy deconvolution

The Richardson-Lucy deconvolution is an iterative method grounded in Bayesian inference principles. Its goal is to enhance the probability that the observed blurred image corresponds to the known Point Spread Function (PSF) [22]. The method follows a specific rule for updating the image with each iteration.

$$I^{(k+1)} = I^{(K)} \cdot \left(\frac{B * h^{\dagger}}{I^{(k)} * h * h^{\dagger}} \right) \tag{1.12}$$

where, PSF is inverted and denoted as, $h^{\dagger}$. The procedure is repeated until it stabilizes, resulting in an estimate of the initial image that is most likely to be accurate, as indicated in source. In simpler terms, this algorithm repeatedly refines and improves edges, which helps restore fine details and sharp transitions in images. This method uses Bayesian statistics to improve the estimated image and PSF by maximizing the likelihood of the observed data. This probabilistic approach is effective for handling noise in a principled way [56].

This technique is highly efficient for handling Poisson noise, which is common in space imaging applications to improve the sharpness of celestial images [22]. Its effectiveness is notable in addressing Poisson noise, which is commonly found in astronomical observations, thus aiding in the discernment of subtle features in telescope-gathered images, as documented in reference [22].

As in the case of inverse filtering approach, the algorithm can unintentionally make noise more pronounced, particularly in areas with high-frequency details. This happens because each iteration enhances both the desired signal and the unwanted noise, resulting in artifacts in the final restored image. Besides, when this algorithm repeatedly processes an image, it can become computationally demanding, especially for large images or when many

iterations are needed to reach a stable result. Most importantly, Choosing the right number of iterations is crucial. Too few can result in incomplete reconstruction, while too many can introduce noise and unwanted patterns. Establishing a suitable stopping point can be challenging [57].

1.3.3.2. Conjugate gradient methods

Conjugate gradient (CG) techniques address the issue of image deblurring by progressively reducing the quadratic form that corresponds to the model of blurring. These techniques are suitable for problems on a large scale and can be integrated with regularization methods to improve their stability and effectiveness [23].

The conjugate gradient approach aims to reduce the value of the target function through its algorithmic process:

$$min_I(\| B - I * h \|^2) \tag{1.13}$$

by repeatedly refining the solution through conjugate directions, which guarantees a swift and efficient convergence.

Conjugate gradient techniques are extensively utilized in the field of medical imaging, especially for reconstructing images obtained from MRI and CT scans. They contribute to producing reconstructions of superior quality while lessening the computational load, which renders them appropriate for clinical settings that demand rapid and precise image recovery [23].

CG methods work well for large, sparse systems. They do not need to store the entire matrix or perform extensive matrix operations, which makes them useful for high-dimensional data problems. For matrices that are symmetric, positive-definite, and well-behaved, CG methods can converge in fewer iterations. The number of iterations is roughly proportional to the square root of the matrix's condition number. This efficiency makes CG faster than traditional methods like Gaussian elimination [58].

CG methods work best with matrices that are symmetric and positive-definite. If the matrix does not meet these conditions, the method might not work well or take longer to converge [58]. To use Conjugate Gradient (CG) methods effectively, you need to think about

numerical stability and efficiency. Dealing with problems like breakdowns or the need for preconditioners can make the implementation more complex.

1.3.4. Iterative methods

Iterative deblurring techniques enhance the approximation of the initial image by continuous revisions, frequently merging concepts from both linear and nonlinear approaches.

1.3.4.1. Iterative blind deconvolution

Iterative blind deconvolution is a process that oscillates between deducing the PSF and the authentic image, progressively honing both predictions. This method is apt for situations where the PSF is not fully determined or is unknown. Commonly, the iterative method includes reducing a cost function that quantifies the variance between the blurred image and the convolution of the estimated image with the PSF [18].

The iterative method can be characterized:

$$\mathrm{I}^{(\mathrm{k}+1)} = \arg\min_{\mathrm{I}} \left(\| \mathrm{B} - \mathrm{I} * \mathrm{h}^{(\mathrm{k})} \|^2 + \lambda R(\mathrm{I}) \right) \tag{1.14}$$

$$\mathrm{h}^{(\mathrm{k}+1)} = \arg min_{h} \left(\| B - I^{(k+1)} * h \|^2 + \mu R(h) \right) \tag{1.15}$$

as a systematic procedure that updates the solution step by step. *R* is the regularization term [18].

Iterative blind deconvolution proves to be highly beneficial in scenarios where the blurring attributes are intricate and defy straightforward modelling, like in everyday photography and video recording. This technique plays a crucial role in restoring clarity to images and videos that are affected by motion blur, thereby improving the overall visual experience of the content [18].

IBD requires a lot of computer processing because it involves repeating steps for estimation and updating. This can take a long time, especially when working with large images or needing many iterations to reach a solution. When using IBD, it is important to be cautious because the iterative process might not always find the best solution. Properly

starting the process and designing the algorithm can help reduce this risk. Also, the accuracy of the final restored image depends a lot on the initial guesses for the image and the PSF. If those initial estimates are not good, it can cause slow progress and less-than-optimal results [59].

1.3.4.2. Expectation-maximization algorithms

EM algorithms approach image deblurring by considering it a problem of estimating hidden variables. It estimates the missing information and parameters through iterative steps, resulting in reliable estimates even when some data is unavailable. They carry out a series of expectation and maximization steps to iteratively estimate the original image and the PSF. In the expectation step, the algorithms calculate the expected values of the hidden variables based on the current estimates, and in the maximization step, they adjust the estimates to increase the probability of the observed data [24].

The EM algorithm's formulation involves these main steps: In the E-step, it calculates the expected values of the hidden variables,

$$Q\left(I, h \mid I^{(k)}, h^{(k)}\right) = \mathrm{E}[\log p(B \mid I, h)] \tag{1.16}$$

and in the M-step, it seeks to optimize the expected log-likelihood of the observed data.

$$\left(I^{(k+1)}, h^{(k+1)}\right) = \mathrm{argmax}_{I,h} Q\left(I, h \mid I^{(k)}, h^{(k)}\right) \tag{1.17}$$

As the EM algorithm progresses, the likelihood function consistently improves. This ensures that the algorithm eventually reaches a peak value for the likelihood function [24]. In addition to that, this method helps find maximum-likelihood estimates by breaking down complex optimization problems into smaller steps involving expectations and maximization [60]. On the other hand, like in the other estimation methods, poor initialization leads to unexpected results.

Expectation-Maximization algorithms are frequently used in fields like medical imaging and remote sensing. The precise calculation of both the image and the PSF is essential in these areas. EM algorithms assist in enhancing the quality of images in cases

where the PSF is not completely determined, leading to improved diagnostic images and more distinct remote sensing information [24].

1.3.5. Comparative analysis

Selecting a deblurring technique is influenced by several elements, such as the nature of the blur, the amount of noise, available computational power, and the specific needs of the application. Linear approaches like Wiener filtering are known for their computational speed but may not perform well with intricate blurs or high noise levels. On the other hand, nonlinear strategies, especially those that use regularization, are more reliable but also more computationally demanding. Methods based in the frequency domain provide refined solutions for particular blur and noise types, yet they demand meticulous attention to boundary issues and potential artifacts. Iterative techniques, despite being resource-intensive, offer adaptability and sturdiness, which are ideal for complex deblurring tasks.

For blurs that are clearly defined and accompanied by minimal noise, linear methods are the go-to choose. Nonlinear methods stand out when it comes to preserving the finer details of images and managing greater levels of noise. Frequency domain methods are valued for their computational swiftness and ease in addressing certain blur varieties. Iterative methods, particularly those that blend blind and non-blind deconvolution, are the most versatile and robust, catering to real-life situations where the characteristics of the blur may be intricate and not well-known.

Conventional image deblurring techniques are fundamental to the evolution of contemporary image restoration methods. Each technique offers distinct benefits and poses specific challenges, making the comprehension of these foundational methods essential for the creation of sophisticated deblurring algorithms. It is anticipated that future research will concentrate on composite methods that merge the advantages of various techniques and utilize machine learning to advance deblurring capabilities.

Progress in computational capabilities and algorithm refinement is poised to catalyse the formulation of more potent and efficient deblurring methods. The amalgamation of time-honoured techniques with modern methodologies, such as deep learning, holds the promise of substantial enhancements in both the quality and practicality of image restoration.

1.4. Point Spread Function Estimation

Estimating the Point Spread Function (PSF) is a critical step in image restoration, serving to define the blur impacting an image. The PSF in image processing illustrates the dispersion of a point light source, like a star in astronomical imagery, within an image due to the imaging system's influence. Factors such as lens flaws, movement, and atmospheric interference can cause this spread [17]. Determining the PSF is vital for reversing this blur and reinstating the image's original clarity. Accurate PSF estimation is pivotal for several reasons such as; image restoration, enhancement of image details and pre-processing. PSF estimation methods are generally divided into two categories: non-blind and blind techniques [17].

1.4.1. Non-Blind PSF estimation

Non-blind PSF estimation operates on the premise that there is pre-existing knowledge about the PSF. This information may be derived from an understanding of the imaging system or through the use of calibration images.

When the type of blur is identified, such as Gaussian or motion blur, the PSF can be characterized through analytical formulas. For example, a Gaussian blur is typically expressed by a specific mathematical function:

$$h(x,y) = \frac{1}{2\pi\sigma^2} exp\left(-\frac{x^2+y^2}{2\sigma^2}\right) \tag{1.18}$$

where σ is the standard deviation [17].

Calibration techniques utilize established test patterns or specific point sources to directly ascertain the PSF. In the context of microscopy, for instance, fluorescent beads serve as a means to gauge the PSF [26].

1.4.2. Blind PSF estimation

Blind PSF estimation operates without any preconceived notions regarding the PSF. It concurrently deduces the PSF and the underlying sharp image directly from the given blurred image.

These algorithms systematically improve the estimates of the PSF and the latent image through iteration. A widely used method is the Richardson-Lucy algorithm, which repeatedly

enhances the estimated image and PSF by adhering to the principles of maximum likelihood [22].

Optimization based techniques approach PSF estimation by treating it as a problem of optimization, aiming to reduce the discrepancy between the observed blurred image and the convolution of the estimated PSF with the latent image [22]. To promote specific characteristics like the PSF's smoothness or sparsity, regularization terms are frequently incorporated into the optimization equation in (1.14, 1.15).

Precise determination of the blurring effect and estimation of PSF allows for the retrieval of clear images and bolsters the efficiency of numerous image processing operations. Ongoing progress in the methods used for PSF estimation is expected to broaden their use and improve their impact across various disciplines for instance medical imaging, astronomy and photography.

1.5. REDS Dataset

The REDS dataset, standing for Realistic and Diverse Scenes, is a high-caliber collection specifically curated for tasks such as image and video deblurring, super-resolution, and other related computer vision activities [25]. Owing to its lifelike scenarios and extensive range of parameters, this dataset is extensively employed for the evaluation and development of algorithms. The document offers an in-depth overview of the REDS dataset, delineating the variety of images it encompasses along with their respective parameters.

The REDS dataset is composed of two main elements: images and videos. Each element is designed to aid various research areas within image and video processing.

The imagery section of the REDS dataset features a wide array of scenes photographed under various circumstances. It covers both interior and exterior settings, different levels of illumination, and a multitude of objects. High-definition cameras are employed to take these images, which is vital for maintaining the intricate details necessary for operations like deblurring and enhancing resolution [25].

The video segment of the REDS dataset comprises frame sequences that depict active scenes with motion blur, camera shake, and various authentic distortions. These sequences are especially valuable for the creation and evaluation of video deblurring and super-resolution algorithms. Accompanying each video sequence is ground truth data, which offers pristine, clear images for comparison [25]. Altogether, the REDS dataset encompasses 300

video sequences, which include 240 for training, 30 for validation, and 30 for testing. Each sequence is made up of 100 frames, culminating in a grand total of 30,000 frames throughout the dataset [25].

The REDS dataset, which includes both images and videos, is distinguished by key attributes that bolster its value for research and development purposes. The images and video frames within the REDS collection are recorded at high resolutions, often exceeding 1920x1080 pixels [25]. This high resolution is critical for assessing the efficacy of algorithms aimed at improving image clarity and retrieving intricate details. In terms of videos, the frame rate is a crucial aspect. The REDS dataset features videos recorded at a rate of 30 frames per second (fps), ensuring fluid motion conducive to the analysis of temporal consistency in video processing algorithms [25]. The dataset encompasses a spectrum of motion blur levels, mirroring situations encountered in the real world where camera or subject movement occurs. This feature is especially useful for the testing and refinement of deblurring algorithms. Additionally, the REDS dataset spans a broad array of lighting conditions, ranging from brightly illuminated outdoor scenes to poorly lit indoor spaces. This diversity is instrumental in evaluating the resilience of algorithms across various lighting situations.

As a resource for the computer vision field, the REDS dataset provides high-quality images and videos with a wide range of parameters, making it an indispensable tool for the development and assessment of image and video processing algorithms.

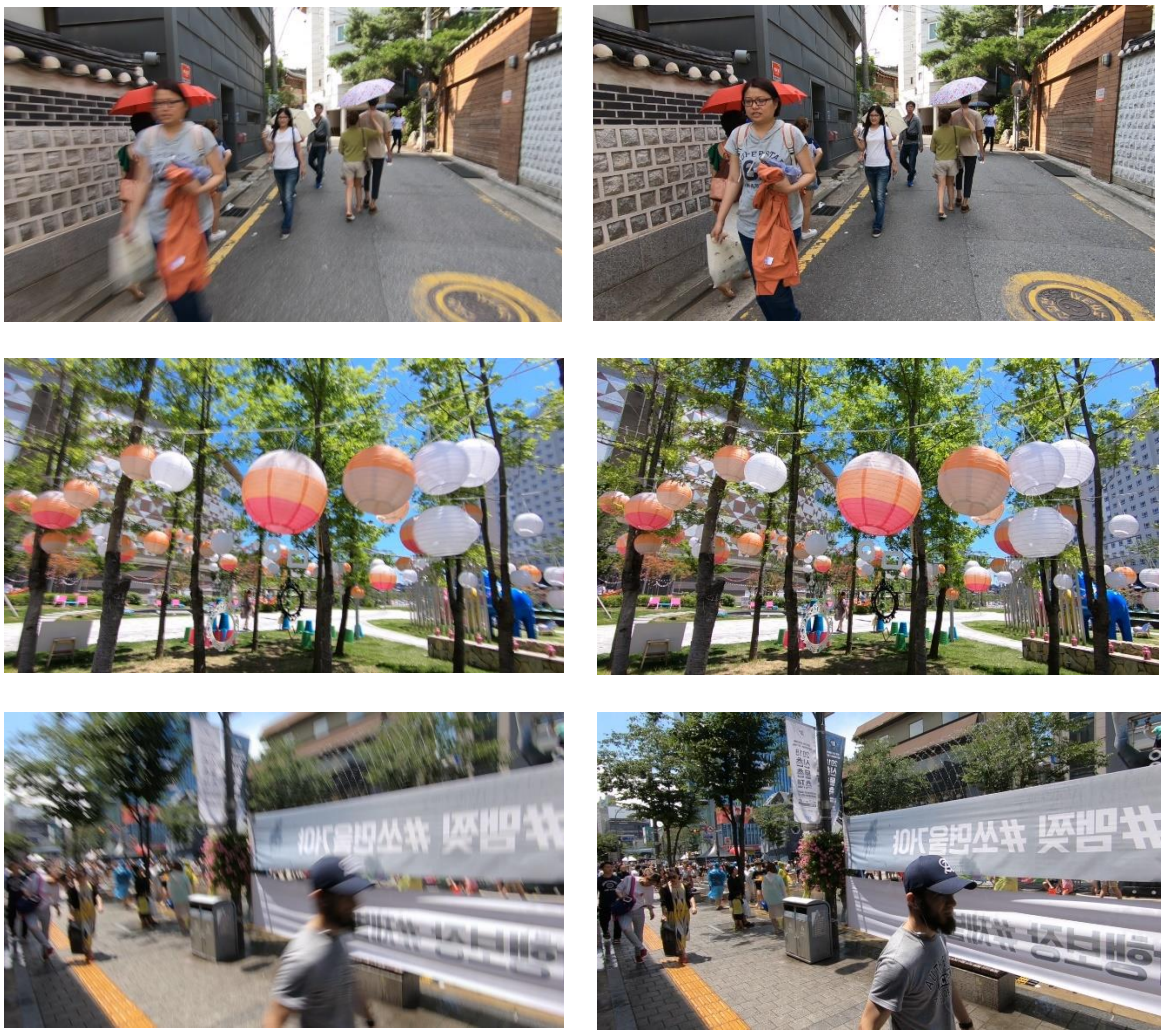

Figure 1.9. Sample blur(left) and sharp(right) images from REDS Dataset

1.6. Proposed Approach

This thesis tackles the challenge of blind image deblurring resulting from linear motion blur. The suggested method is structured into three principal stages: estimating the PSF, restoring the image, and assessing the method's effectiveness. It employs a straightforward method for estimating the PSF within the frequency domain, which is then paired with Wiener deconvolution. The objective is to create a method that is both effective and reliable for reconstructing images affected by linear motion blur, a prevalent problem in numerous imaging scenarios.

The initial stage of the proposed method is dedicated to determining the parameters of the Point Spread Function (PSF), particularly the extent and orientation of the motion blur, by employing frequency domain strategies. Precise estimation of the PSF is imperative for

successful deblurring. This technique takes advantage of the unique patterns that motion blur creates in the frequency domain [27], [28].

Following the estimation of the PSF, the subsequent step is the reconstruction of the blurred image through Wiener deconvolution. This method is chosen for its proficiency in harmonizing noise attenuation with image sharpening, thereby yielding images of superior quality. During this phase, the Wiener filter is employed, capitalizing on the predetermined PSF to counteract the linear motion blur's impact [17].

The concluding stage encompasses the appraisal of the devised method's efficacy. This assessment employs a variety of indicators, such as the Peak Signal-to-Noise Ratio (PSNR), Mean Square Error (MSE) and the Structural Similarity Index (SSIM), to gauge the fidelity of the reconstructed images. The method under consideration is subjected to trials using the REDS dataset images, which serves as a stringent standard for comparing image deblurring algorithms.

2. THEORY

2.1. Image Formation Model

In the study of blind image deblurring, the image formation model is essential to grasp how images are captured and then deteriorated by several elements, such as motion blur. This part offers an in-depth analysis of the image formation model, highlighting two essential components: the procedure of capturing images and the convolution method that leads to image deterioration.

2.1.1. Image acquisition process

The process of image acquisition refers to the methods through which a scene is recorded and transformed into a digital image. It includes how light interacts with the scene, the camera's optical system, and how the sensor reacts to these elements.

2.1.1.1. Light interaction and optical system

Light from a scene is directed through the camera's lens, which then focuses it onto the sensor. The characteristics of the lens, such as its aperture, focal length, and optical imperfections, can cause blurring. The PSF defines how the optical system reacts to a single

light point, encompassing the blur caused by the lens, which is a significant factor in the overall blur seen in the final image [29].

The lens's aperture size, or f-stop, determines the quantity of light that enters the camera and influences the depth of field. A wider aperture lets in lighter but narrows the depth of field, making parts of the image blur. A smaller aperture widens the depth of field but may increase motion blur if there's movement during the shot due to longer exposure times [29].

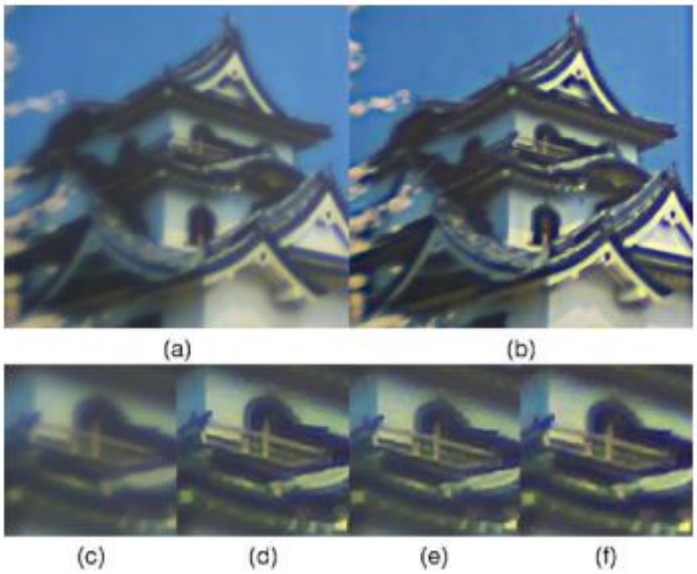

Figure 2.1 (a) original blur image due to lens (b) deblurred image (c)original blurred image (d) (e) (f)images with deblurred using different models [62]

Optical aberrations like spherical aberration, chromatic aberration, and astigmatism lead to flaws in image formation. Spherical aberration happens when light passing through the lens edges focuses differently than light through the centre, blurring the image's edges. Chromatic aberration is when the lens fails to focus all colours at one point, creating colour fringes around objects. Astigmatism makes light points look like lines, varying with their orientation to the lens [29].

The PSF is vital for modelling and correcting blur caused by the lens. It is usually shown as a two-dimensional function that illustrates how light from a point source spreads in the image plane. The PSF can be determined through experiments or estimated with methods like deconvolution algorithms, which try to undo the blur by approximating the PSF [13].

2.1.1.2. Sensor response

The sensor, usually a CCD or CMOS type, transforms the focused light into an electric signal. Factors such as the sensor's resolution, sensitivity, noise traits, and the color filter array contribute to how the image is formed. This analog signal is then converted into a digital format, which can cause quantization effects. The value of each pixel in the image that is produced reflects the combined impact of the light's intensity and the sensor's reaction throughout the duration of the exposure [29].

CCD sensors, which stand for Charge-Coupled Device, are recognized for producing high-quality images with minimal noise. They function by changing light into an electrical charge and moving this charge to a readout section. There, it is turned into a voltage, boosted, and finally digitized. Due to their high-quality image output, CCD sensors are preferred in professional-grade cameras, although they tend to be costlier and consume more power than their CMOS counterparts.

CMOS sensors, short for Complementary Metal-Oxide-Semiconductor, combine the photo-detection and readout electronics on a single chip, which enables quicker data retrieval and reduced energy usage. These sensors are typically found in standard consumer cameras and portable gadgets. Despite this, they may experience greater noise and not match the image quality of CCD sensors. Nonetheless, CMOS technology has seen considerable enhancements, elevating their performance to a level appropriate for various uses [29].

The sensor's resolution, which is the pixel count, dictates the detail level that the sensor can record. Sensors with a higher resolution can detect more subtle details, but they demand greater processing capability and more storage. The sensitivity of the sensor, also known as the ISO rating, reflects its capacity to take pictures in dim lighting. Using higher sensitivity settings boosts the sensor's light detection but can also heighten noise, resulting in images with more grain.

Digital image noise originates from different sources such as thermal noise, shot noise, and readout noise. Thermal noise is linked to the random movement of electrons in the sensor and grows with rising temperature and longer exposure times. Shot noise is a natural part of detecting photons and is described by a Poisson distribution. Readout noise occurs during the sensor's data retrieval phase and its extent can differ based on the sensor's architecture and its electronic components.

The color filter array (CFA) plays a role in recording color details in digital images. The Bayer filter is the most prevalent CFA design, consisting of a mosaic pattern of red,

green, and blue filters. A color filter is placed over each pixel, and algorithms known as Demosaicing are used to interpolate the absent color data from nearby pixels. The selection of the CFA design and the Demosaicing technique can have an impact on the image's color fidelity and overall quality [13].

2.1.1.3. Exposure time and motion blur

When the camera and the scene move relative to each other during the time the camera's shutter is open, motion blur occurs. This type of blur depends on how long the shutter is open and the path of the movement. In cases of straight-line motion blur, the image appears to be dragged out in the movement's direction, with the amount of blur being directly related to the motion's speed and how long it lasts. Mathematically, this effect is represented as a convolution of the original, clear image with a linear PSF.

The exposure time, also known as shutter speed, sets how long the sensor is open to light. Extended exposure times mean more light can hit the sensor, which helps in darker settings but also raises the chance of motion blur. On the other hand, shorter exposure times lessen the likelihood of motion blur but necessitate the use of higher sensitivity or bigger apertures to achieve the right exposure level.

Motion blur happens when movement between the camera and the scene smears the image in the direction of that movement. This smearing can be due to the camera moving, the subject moving, or both. With linear motion blur, the image looks elongated in a straight path, and the amount of blur relates to how fast and how long the movement is. The PSF for this kind of blur is usually depicted as a consistent line shape that matches the motion's direction, defined by its length and orientation [30].

Motion blur can greatly reduce the clarity of an image, complicating the recognition and understanding of small details. To correct motion blur, it is necessary to determine the PSF and use deblurring methods to restore the sharpness of the image. Precise PSF estimation is vital for successful deblurring. There are several techniques suggested for estimating the PSF from blurred images, such as edge detection, analysis in the frequency domain, and approaches based on traditional algorithms and machine learning [18].

2.1.2. Convolutional model for image degradation

The convolution model is a mathematical method used to describe how an image gets blurred. Specifically, for linear motion blur, the blurred image we see, denoted as, Ib, is

understood as the result of combining the original sharp image, Is, with the PSF, h, and then adding noise, n.

2.1.2.1. Mathematical formulation

The impaired image, Ib, can be mathematically represented as follows:

$$Ib(x,y) = \big(Is * h(L,\theta)\big)(x,y) + n(x,y) \tag{2.1}$$

Here, the symbol, *, signifies the convolution process, and (x, y) are the coordinates in space. The PSF, h, for linear motion blur is generally depicted as a straight line that's consistent with the motion's path, defined by its length L and its angle θ [31].

The convolution operation blends the distinct image, Is, with the PSF, h, which produces a blurred image. This action can be pictured as the PSF extending the brightness of each pixel in the distinct image to the surrounding pixels, leading to the typical streaking seen in images affected by motion blur. The extra noise, n, symbolizes the collective impact of different noise sources, such as those from the sensor, quantization, and external environmental factors.

2.1.2.2. Frequency domain representation

In the spatial domain, convolution is equivalent to multiplication in the frequency domain. By applying the Fourier transform,

$$Fb(u,v) = Fs(u,v) \cdot H(u,v) + N(u,v) \tag{2.2}$$

Fb, Fs, and H are the Fourier transforms of Ib , Is , and h, respectively, and (u, v) refer to positions in the frequency domain. This way of representing the data makes it easier to work with blurred images, as the process of deconvolution, which is used to sharpen images, can be done more effectively in the frequency domain [7].

The Fourier transform breaks down an image into its constituent frequencies, where low frequencies correspond to gradual changes and high frequencies to detailed aspects. Within the frequency domain, the act of convolution is simplified to multiplication, which facilitates more streamlined calculations. The frequency response of the PSF, $H(u, v)$, functions as a filter that diminishes specific frequency elements, leading to the distinctive blur in the image.

Representing an image in the Fourier domain aids in applying different image processing methods like filtering, restoring, and improving the image. By adjusting the frequency elements, one can target and refine or diminish particular attributes of the image. This assists in processes like identifying edges, minimizing noise, and sharpening blurred images [17].

2.1.2.3. Noise considerations

Noise in an image is often represented as additive Gaussian noise. This type of noise mainly affects the image's high-frequency details, making the deblurring task more challenging. Successful deblurring methods, like Wiener deconvolution, take into account the properties of noise to find a middle ground between making the image clearer and reducing the increase of noise.

Additive Gaussian noise is described by its mean and variance. The values of this noise type are distributed normally. The mean is the average level of noise, and the variance shows how strong the noise is. Usually, this noise is considered to have a zero mean, which makes it easier to analyse and model.

In the realm of image processing, elements of an image that have high frequency are linked to intricate details and abrupt changes, like edges and surface patterns. These elements are more susceptible to the effects of noise because the random variations that noise introduces might be confused with actual high-frequency information. When attempting to deblur an image by enhancing these high-frequency elements to regain clarity, there is a risk of also increasing the noise, which can result in unwanted distortions.

Successful methods for deblurring should consider the specific properties of noise to prevent excessive enhancement of noise during the process of sharpening the image. This consideration becomes crucial when there is a significant amount of noise, as it requires a balance between improving image sharpness and reducing noise to produce an image that is aesthetically satisfactory [13].

2.2. Linear Motion Blur

Linear motion blur is an important aspect of image processing that greatly influences the sharpness and definition of images taken when there is movement between the camera and the subject. Grasping the concept of linear motion blur is vital for creating successful deblurring algorithms. This section delves deeply into linear motion blur, concentrating on two key elements: the idea of the PSF and its impact on motion blur, and the mathematical

depiction of the motion blur kernel. Also, as it is seen from the picture below, motion blur also effects the histogram of images [67]. As motion blur degree increases, histogram of image transform to a triangular shape.

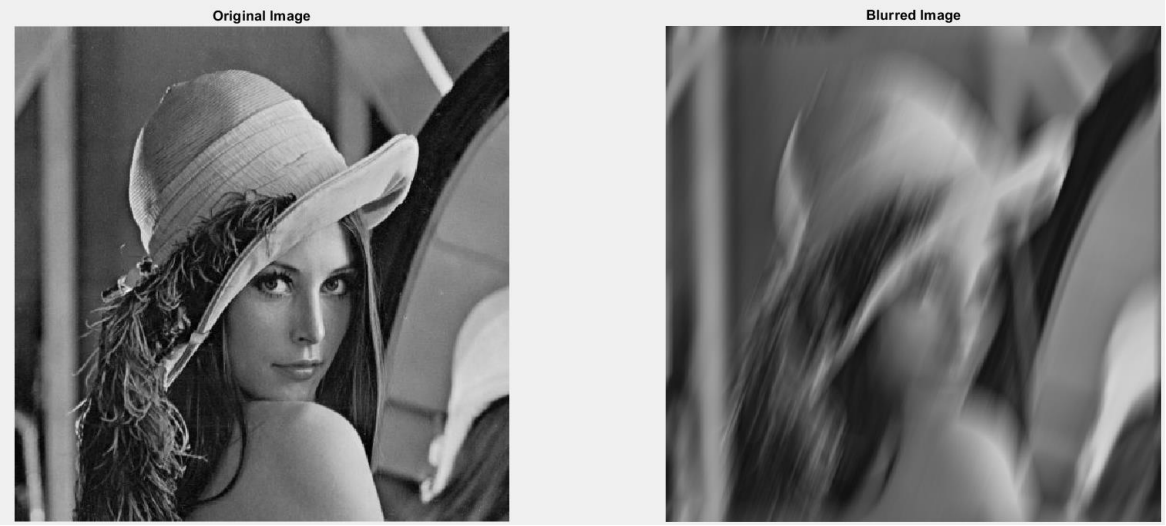

Figure 2.2. Original Lena image and linear uniform motion blurred Lena image

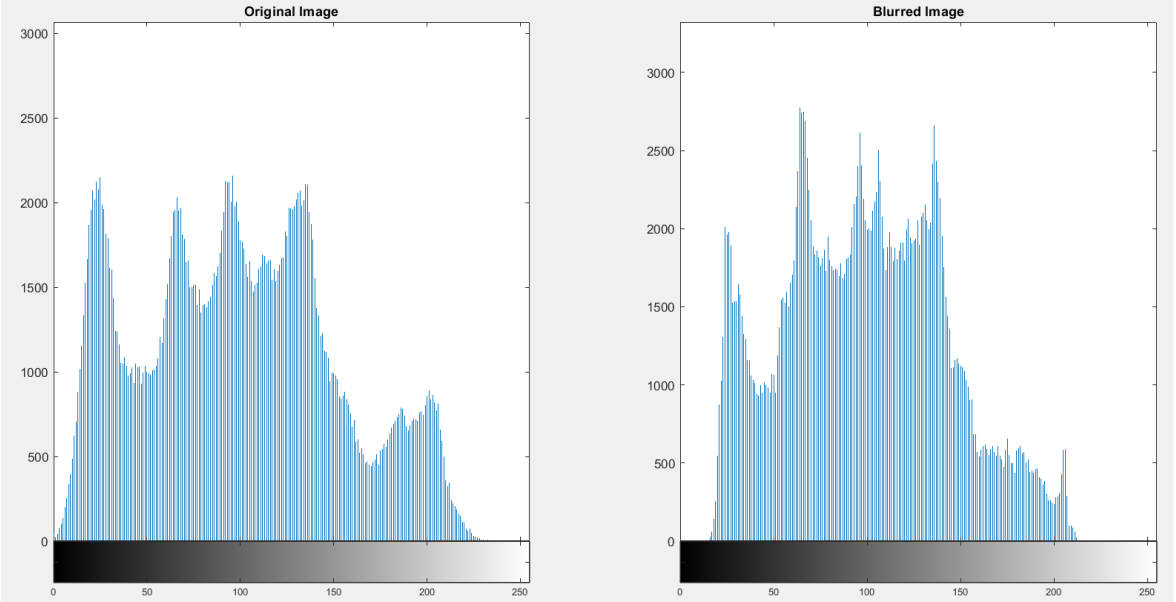

Figure 2.3. Histogram of original Lena image and histogram of linear uniform motion blurred Lena Image

2.2.1. PSF concept and its role in motion blur

The point spread function is a key element in optical imaging, which characterizes how the system reacts to a single point of light. It is essential for comprehending and formulating the impact of linear motion blur in imaging.

2.2.1.1. Definition and characteristics of PSF

The point spread function characterizes how an optical imaging system responds to a point source or point object. Ideally, a point source would be imaged as a single point, but due to imperfections and physical constraints, the resulting image shows a blurred spot. The shape and extent of this spread depend on factors like lens aberrations, diffraction, and, foremost, motion during exposure [29].

In the context of linear motion blur, PSF takes the form of a line segment. This PSF represents the trajectory of a point source during the camera's exposure time. Specifically, the length of the line segment corresponds to the distance travelled by the point source, while its orientation indicates the direction of motion. This simplification assumes uniform motion, which is a practical approximation in many real-world scenarios [13].

2.2.1.2. Role of PSF in motion blur

PSF is crucial in understanding motion blur in images. When a camera moves relative to the scene during exposure, each point in the scene projects a line segment onto the image plane instead of a single point. The resulting observed image is a convolution of the sharp (latent) image with the PSF, leading to a blurred image. The extent and direction of the blur depend on the motion characteristics [30].

Equation (1.18) gives the mathematical representation of PSF description. When we convolve a sharp image with the PSF, each pixel in the original image affects multiple pixels in the blurred version. It's like spreading the details along the motion path [18].

2.2.1.3. Estimating the PSF

Estimating the PSF is vital step for effective image deblurring. Researchers have proposed various methods for PSF estimation, spanning from analytical approaches to data-driven techniques. Analytical approaches rely on mathematical analysis. Imagine the PSF as a "blur recipe." Analytical approaches often involve edge detection and frequency domain analysis. By doing so, we can infer the PSF's parameters, such as its length L and orientation θ [7].

Edge detection and gradient methods, in the realm of blind image deblurring, focus on estimating PSF by analyzing edge profiles within the blurred image and considered as analytical proposition to the problem. These approaches leverage the gradients of edges to extract information about the blur direction and extent. For instance, the Radon transform

has been employed to estimate motion blur direction by detecting lines in the frequency domain [18].

In the frequency domain analysis, the motion blur PSF exhibits characteristic patterns, including zero crossings within the frequency spectrum. By analyzing these patterns, we can infer the PSF parameters. For instance, the Cepstrum analysis method utilizes the logarithm of the Fourier transform to detect periodic structures caused by the PSF. Frequency domain analysis method viewed as both analytical and data-driven solution to the estimation problem.

Blind deconvolution methods jointly estimate the latent image and the PSF considered as both analytical and data driven technique depending on the specific approach. These techniques typically rely on iterative optimization, where the image and PSF are alternately updated to minimize a cost function. Regularization terms are incorporated to ensure stable solutions and to integrate prior knowledge related to either the image or the PSF.

The accuracy of estimating the PSF significantly impacts the effectiveness of deblurring algorithms. When the PSF estimation is inaccurate, the resulting deblurred images may exhibit artifacts such as incompleteness or excessive sharpening. Therefore, robust techniques for PSF estimation are essential to adapt to various blur characteristics.

2.2.2. Mathematical representation of motion blur kernel

In this section, we delve into an intricate mathematical representation of motion blur kernels. Understanding these kernels is pivotal for comprehending the impact of motion blur on images and for devising effective deblurring techniques. The PSF characterizing linear motion blur is conventionally expressed as a mathematical function that delineates the intensity distribution of a point source during its rectilinear trajectory and can be expressed as:

$$PSF(x,y) = \frac{1}{L} \cdot rect\left(\frac{xcos\theta + ysin\theta}{L}\right) \cdot \delta(xsin\theta - ycos\theta) \tag{2.3}$$

where L is the length of blur in pixels, θ is the angle of the motion blur relative to the horizontal axis, δ is the Dirac delta function and *rect* is the rectangular function defined as:

$$rect(u) = 1, |u| \leq 0.5$$
$$rect(u) = 0, otherwise \tag{2.4}$$

The intensity distribution along the motion path is mathematically modelled as uniform, a widely used approximation for linear motion blur [32].

2.3. Frequency Domain Analysis

In image processing, frequency domain image analysis provides powerful tools for capturing and modifying image properties, particularly for blurring tasks. This section explores the fundamental ideas behind the techniques used in this work: the Fourier transform concept and the frequency spectrum properties of blurred images.

2.3.1. Fourier transform concept

An image or signal in the spatial domain can be converted to its frequency domain representation using a mathematical technique called Fourier transform. Since many images processing tasks such as filtering and blurring is performed more effectively in the frequency domain, this transformation is essential for image processing.
The 2D Fourier transform of an image *f(x,y)* is defined as:

$$F(u,v) = \int_{-\infty}^{\infty}\int_{-\infty}^{\infty} f(x,y)e^{-j2\pi(ux+vy)}dxdy \tag{2.5}$$

f(x,y) is images spatial domain representation, *F(u,v)* is representation in frequency domain, *u* and *v* are variables in frequency domain, *j* is the imaginary unit.

The inverse Fourier transform, which reconstructs the spatial domain image from its frequency domain representation, is given by:

$$f(x,y) = \int_{-\infty}^{\infty}\int_{-\infty}^{\infty} F(u,v)e^{j2\pi(ux+vy)}dudv \tag{2.6}$$

The most important properties of the Fourier transform include linearity, shift and convolution theorem. The Fourier transform of a sum of functions is the sum of their Fourier transforms which supports linearity property. A shift in the spatial domain corresponds to a phase shift in the frequency domain. Convolution in the spatial domain corresponds to the multiplication in the frequency domain. These properties are particularly useful for image processing tasks. For example, the convolution theorem simplifies the

complex convolution operation in the spatial domain into a simple multiplication in the frequency domain [13].

Fourier transform is widely used in image processing for tasks such as filtering, image enhancement and blurring. In the context of motion blur, the transformation allows the blur to be represented as a function in the frequency domain, thus simplifying the deblurring process. The importance of the Fourier transforms in image blurring is highlighted by its ability to convert the complex convolution operation in the spatial domain into a simple multiplication in the frequency domain, making it computationally efficient [17].

To enhance image deblurring, a valuable approach involves converting the PSF into the frequency domain. This conversion simplifies the convolution process, replacing it with element-wise multiplication thereby, deblurring operation becomes computationally easy and effective.

2.3.2. Frequency spectrum of blurred images

Understanding the frequency spectrum of blurred images is critical to developing effective deblurring algorithms. When an image is blurred due to linear motion, its frequency spectrum has specific properties that can be used to restore.

The frequency spectrum of an image is affected in predictable ways by linear motion blur. In the frequency domain, the motion blur PSF is represented by a sine function. A linearly blurred image can be described by its frequency response as follows.

$$H(u,v) = \frac{\sin(\pi(ucos\theta + vsin\theta)L)}{\pi(ucos\theta + vsin\theta)L} \tag{2.7}$$

Suppose that the motion is along the x-axis, and the PSF is defined as:

$$h(x,y) = \frac{1}{T} rect\left(\frac{x}{T}\right)\delta(y) \tag{2.8}$$

$$rect\left(\frac{x}{T}\right) = \begin{cases} 1, & if\ |x| \le \frac{T}{2} \\ 0, otherwise \end{cases} \tag{2.9}$$

Length of the motion blur is expressed as T. Taking the FT of PSF:

$$F\{h(x,y)\} = H(f_x, f_y) = \int_{-\infty}^{\infty}\int_{-\infty}^{\infty} h(x,y)e^{-i2\pi(f_x x, f_y y)}dxdy \tag{2.10}$$

$$H(f_x, f_y) = \int_{-\infty}^{\infty}\int_{-\infty}^{\infty} \frac{1}{T} rect\left(\frac{x}{T}\right)\delta(y)dy \tag{2.11}$$

To simplify the integral, examine the existence of the delta function δ(y) which is the integral over y is effectively picking out the value at y=0. So, double integral can be made easy by taking single integral over x.

From Equation (2.11), limits of the integral can be converted to:

$$H(f_x, f_y) = \int_{-\frac{T}{2}}^{\frac{T}{2}} e^{-i2\pi(f_x x)}dx \tag{2.12}$$

$$H(f_x, f_y) = \frac{1}{T}\left[\frac{e^{-i2\pi f_x \frac{T}{2}} - e^{i2\pi f_x \frac{T}{2}}}{-2\pi f_x}\right] \tag{2.13}$$

$$H(f_x, f_y) = \frac{1}{T}.\frac{2\sin(\pi T f_x)}{2\pi f_x} \tag{2.14}$$

$$H(f_x, f_y) = \frac{\sin(\pi T f_x)}{\pi T f_x} \tag{2.15}$$

$$H(f_x, f_y) = sinc(T, fx) \tag{2.16}$$

As a result of equation (2.16), when an image is blurred due to motion in a straight line (like a camera shake), its frequency representation shows a specific pattern called a sinc function. Understanding this helps in tasks like removing motion blur from images [13], [49].

In the domain of frequency analysis, the sinc function generates a sequence of zeros and oscillations. The key results include attenuation of high frequencies, directional characteristics, repetition and aliasing. The motion blur results in a notable reduction of high-frequency components, which are associated with intricate features and boundaries present

in the image. The orientation of motion blur can be observed in the frequency domain. The angle θ of motion blur plays a crucial role in defining the alignment of the zeros and oscillations of the sinc function. Owing to the periodicity exhibited by the sinc function, the frequency spectrum of a blurred image displays recurring patterns, which may give rise to aliasing.

These essential traits play a crucial role in the frequency domain examination of blurred images. Through comprehension of these patterns, deblurring algorithms are able to pinpoint the particular frequency elements impacted by the blur [32].

Frequency domain methodologies for image deblurring capitalize on the expected influence of motion blur on the spectral characteristics of the image. An illustration of this concept is found in Wiener deconvolution, which makes use of the established frequency behaviour of the blur PSF to recover the initial image. The Wiener filter, when implemented in the frequency domain, seeks to reverse the influences of blurring while concurrently reducing the influence of noise as in equation (1.6). This process of filtering effectively counteracts the influence of blurring on the frequency spectrum, leading to the restoration of high-frequency elements and enhancement of the image.

2.4. Frequency Spectrum Analysis for PSF Estimation

Accurate estimation of the PSF is essential for achieving optimal results in the process of image deblurring. The following section delves into an examination of the characteristics of the frequency spectrum when subjected to motion blur, as well as methodologies for determining blur parameters specifically angle and length from said spectrum.

2.4.1. Properties of the frequency spectrum under motion blur

The occurrence of linear motion blur within an image result in the emergence of unique characteristics within its frequency spectrum. It is imperative to comprehend these characteristics in order to accurately estimate the Point Spread Function. The frequency domain depiction of linear motion blur, as mentioned earlier, is defined by a sinc function. The roots of this function are associated with distinct frequency elements that are fully suppressed by the blur.

The principal effect of motion blur on the frequency spectrum involves attenuation of high frequencies and directional patterns. The decrease in high-frequency elements causes blurring in the image due to the representation of intricate details. The motion blur's alignment in the frequency domain generates spatial orientations, correlating with the blur's

direction. These characteristics are employed for the calculation of the PSF parameters, such as the extent and orientation of the motion blur [28].

Figure 2.4. Image without motion blur and its Fourier spectrum [28]

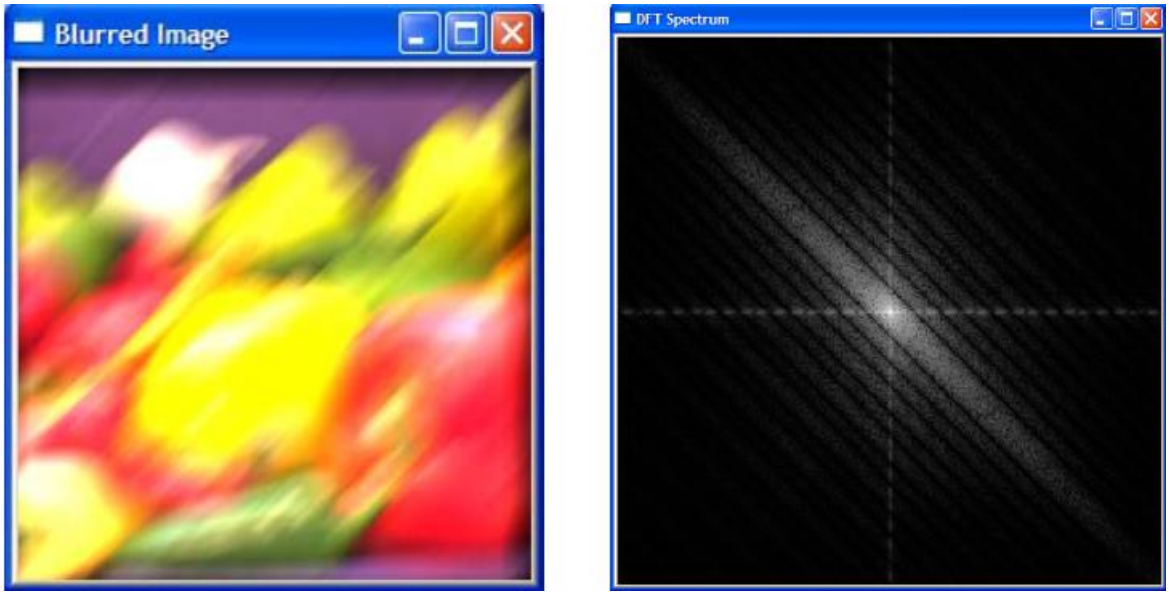

Figure 2.5. Motion blurred image with θ =45° and L=31 pixels and its Fourier spectrum [28]

2.4.2. Logarithmic transformation

When logarithmic transformation is applied to an image, we're adjusting the pixel values to enhance certain features. The magnitude of the Fourier transform of an image frequently includes several orders of magnitude. High-frequency component of the image can be importantly smaller than low-frequency components of the image. LT can be defined

as below, here, I is image, and F(I) is the FT of image [13]:

$$F_{\log}(I) = \log(1 + |F(I)|) \tag{2.17}$$

By taking logarithmic transform of FT image, dynamic range is compressed, and allowing for simultaneous, revised visualization of both high and low-frequency components.

The logarithmic spectrum underlines smaller values not larger values, enhancing the visibility of details and patterns that might be covered in a linear scale. This property leads to see the patterns of blur parameters.

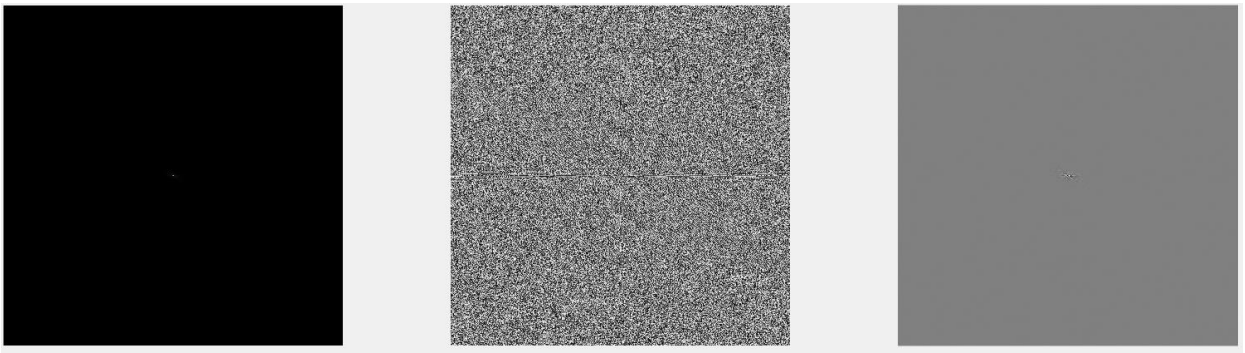

(a) (b) (c)

Figure 2.6. (a) Magnitude (b) Phase (c) Imaginary part of FT image

It can be seen from Figure 2.6 that, blur patterns cannot be seen from FT of image, but parameters are visual seen from LT transformed image.

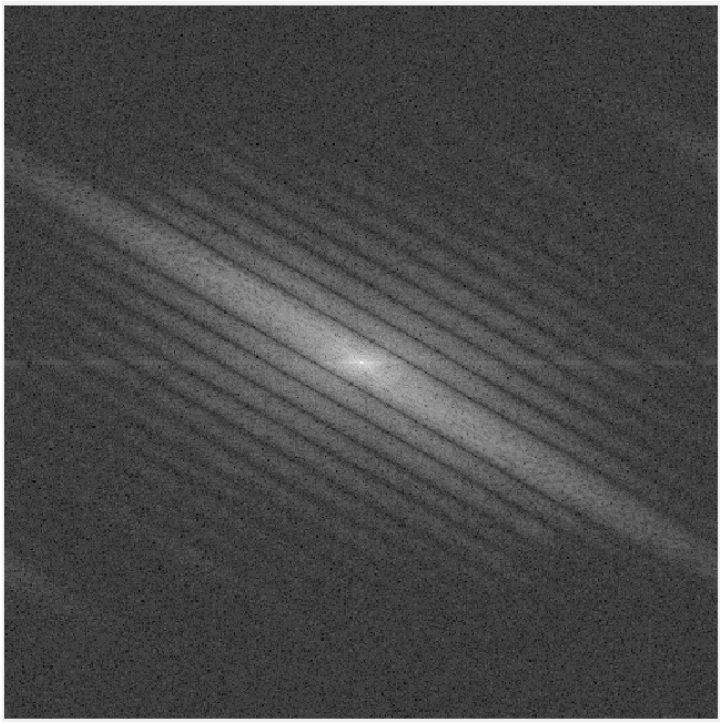

Figure 2.7. Logarithmic Transform of FT image with uniform motion blur

2.4.3. Techniques for extracting blur parameters from the spectrum

Several techniques have been developed to extract blur parameters from the frequency spectrum. These techniques often involve analyzing the directional patterns and frequency attenuation caused by the blur. The blur angle θ can be estimated by analyzing the orientation of the zeros in the frequency spectrum. Techniques such as the Radon transform are commonly used for this purpose. The Radon transform integrates the image along specified directions, highlighting the predominant blur direction.

$$\theta = argmax_{\theta} \int_{-\infty}^{\infty} \int_{-\infty}^{\infty} F(u,v)\delta(ucos\theta + vsin\theta)dudv \tag{2.18}$$

The blur length L is estimated by analyzing the spacing between the zeros of the sinc function in the frequency spectrum. The distance between successive zeros is inversely proportional to the blur length.

$$L = \frac{1}{\Delta u} \tag{2.19}$$

where, Δu is the distance between the zeros in the frequency domain. These techniques

provide a framework for estimating the PSF parameters, enabling effective deblurring using methods such as Wiener deconvolution [7].

2.5. Wiener Deconvolution for Image Restoration

Wiener deconvolution is an effective method for restoring images, considering the degradation function, known as the PSF, as well as the traits of the noise. Its goal is to reduce the mean square error between the reconstructed image and the original image.

2.5.1. Mathematical formulation of the wiener filter

The formula for the Wiener filter, denoted as, $W(u,v)$, is defined to achieve this objective.

$$W(u,v) = \frac{H*(u,v)}{|H(u,v)|^2 + \frac{S_n(u,v)}{S_s(u,v)}} \tag{2.20}$$

In the equation, H^* is the complex conjugate of H, and S_n and S_S denote the power spectral densities of the noise and the original sharp image, respectively. The Wiener filter is designed to balance the process of reducing blur and minimizing noise effectively.

The Wiener filter originates from statistical concepts, focusing on reducing the mean square error between the estimated image and the actual one. It includes the power spectral densities of both the noise and the clear image, allowing it to adjust to the varying frequency attributes of the signal and the noise.

The power spectral density is a measure that shows how the power of a signal is spread across different frequencies. In terms of noise, the PSD, denoted as $S_n(u,v)$, reflects how intense the noise is at various frequencies. For a sharp image, the PSD, represented as, $S_s(u,v)$, describes how the details of the image are distributed over the frequency range. Within the Wiener filter's formula, the fraction $\frac{S_n(u,v)}{S_S(U,V)}$ serves as a control mechanism, often revealed as K, which helps to avoid the overemphasis of frequencies where noise is predominant.

The success of the Wiener filter hinges on the precise determination of the PSF and the noise details. Typically, these factors are deduced from the blurred image that is being observed, employing methods like detecting edges, analyzing autocorrelation, or applying

machine learning techniques. It is essential to estimate these parameters accurately to ensure the deblurring yields results of superior quality.

To encapsulate, the convolution model for image degradation offers a detailed structure for comprehending and tackling motion blur in digital images. By depicting the blur as a convolution process and examining the issue within the frequency domain, we can create potent deblurring strategies that enhance sharpness and control noise increase. The Wiener deconvolution technique is a prime example of this strategy, providing a strong method for eliminating motion blur that considers both the PSF and the noise properties.

2.5.2. Properties and advantages of wiener deconvolution

Wiener deconvolution offers several advantages for image restoration such as noise suppression, optimal restoration and computational efficiency. By incorporating the noise-to-signal ratio, the Wiener filter reduces the amplification of noise, resulting in cleaner restored images. Also, minimizes the mean square error, providing an optimal balance between deblurring and noise suppression. Finally, the filter operates in the frequency domain, leveraging the Fast Fourier Transform for efficient computation. These properties make Wiener deconvolution a preferred choice for image restoration in various applications, including medical imaging, remote sensing, and photography [28].

3. MOTIVATION

In this thesis, blind PSF estimation method applied on uniform motion blurred images. To do so, frequency domain analysis approach employed to determine basis elements of PSF; motion angle and pixel size. Then, blurred image is filtered by using wiener deconvolution technique with calculated PSF parameters. This algorithm is utilized firstly on standard images such as Lena image with given motion angles and pixel sizes. Results of these known image are to measure and compare the success of the algorithm between frequency domain analysis algorithms. Finally, results on images in REDS dataset are compared to current deep learning based deblurring methods. Also, real world application of this study is an important step to analyse and measure applicability.

3.1. Application

There are huge number of studies about blind image deblurring algorithms on motion blurred images. Some of them based on deep learning methods and some of them based on less complex methods.

In this thesis, only less complex and faster frequency domain analysis methods to estimate linear uniform motion blur PSF will be discussed.

3.1.1. Hough transform method to estimate PSF: review on literature and an algorithm

Hough Transform is a vital technique and basically a voting algorithm for edge or shape detection that forms a basis for recognition algorithms in. This method is also useful for uniform linear motion blur images by making motion blur parameters that is blur pixel length and angle detectable in the log spectrum of FFT image. Since HT can easily detect lines or images whether it is straight line or line with breaks, from log spectrum direction and length of the mail lobe can easily be estimated.

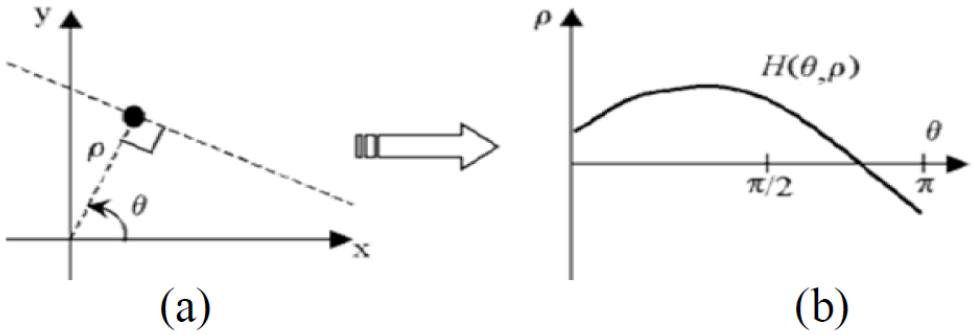

Figure 3.1 Hough Transform parameters (a) x-y pixel space (b) ρ and θ parameter space [37]

In HT, for any pixel (x, y) in image, there is a parameter space (ρ, θ), denoted as,

$$\rho = x\cos\theta + y\sin\theta \tag{3.1}$$

and it reduces line detection problem to point matching problem in parameter space [39].

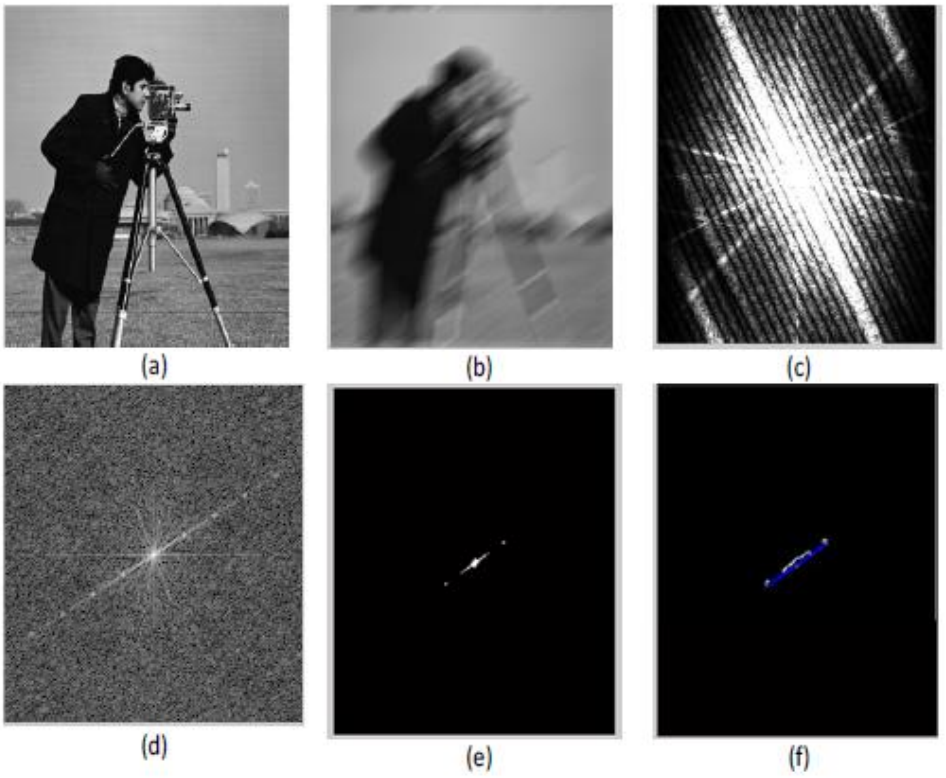

Figure 3.2. HT for extracting motion parameters (a) cameraman image (b) motion blurred image with L=30 pixels and θ=30° (c) log spectrum (d) modified log spectrum (e) fourth bit plane of log spectrum (f) line found by HT [37]

It can be seen from the Figure 3.2 that, HT finds and extracts line and returns

orientation that corresponds to blur angle θ.

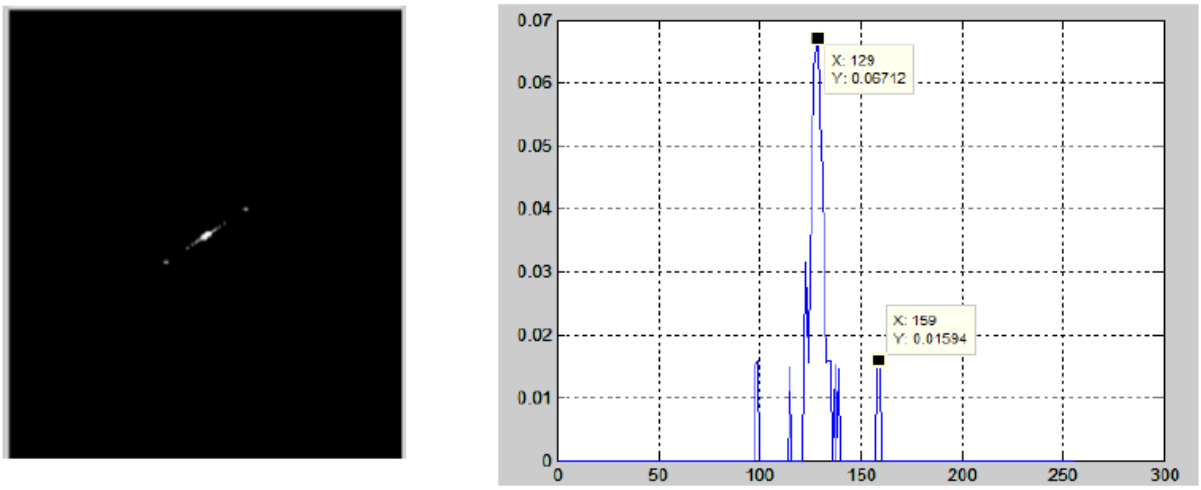

(a) (b)

Figure 3.3. HT L estimation (a) fourth bit-plane of log spectrum image (b) distracting peak points

By taking averages of columns at the image in Figure 3.3, blur length parameter L can be approximated. It is evaluated as the difference between peak points of first and second central lobe in log spectrum of the image.

HT brings the study of dual motion blurs in image that one can find both blur angle and length for spatially variant case [38].

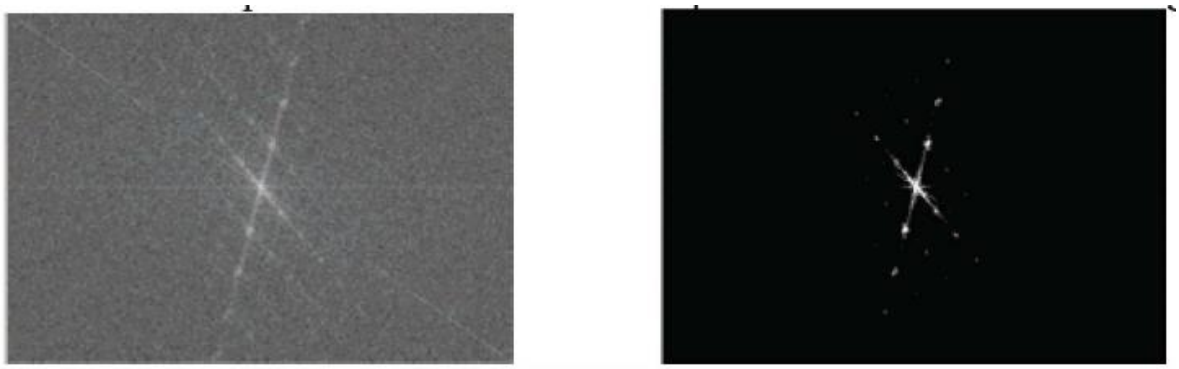

Figure 3.4. HT study for spatially variant image (a) log spectrum (b) fourth bit plane [38]

The pseudocode of HT algorithm to find motion blur angle and length, constructing PSF and deblurring is given below in Table 3.1.

Table 3.1. Algorithm - PSF Estimation with HT and Deconvolution of Blurred Image

1: Convert blurred observed RGB image to gray level image

2: Compute Fourier Transform of gray level image at step 1

3: Calculate log spectrum of FFT gray scale image from step 2

4: To eliminate noise, recalculate step 2 and step 3 to get modified log spectrum

5: Execute bit plane slicing and then extract fourth bit plane of step 4 to better estimate

6: Employ Canny edge detection method to emphasize edges to the output of step 5

7: Apply Hough transform to output of step 6 to estimate blur angle $\boldsymbol{\theta}$

8: Use output of step 3 and rotate it by $\boldsymbol{\theta}$ to the reverse direction

9: Transform output of step 8 that is 2D image to 1D by Averaging the columns of the output of step 8

10: Find L by taking the difference of pixel position according to average values of first peak and second peak from step 9

11: Generate PSF function based on the blur parameters from the output of step 7 and step 10

12: Deconvolve blurred image with Wiener deconvolution by using estimated PSF from the output of step 11

3.1.2. Radon transform method to estimate PSF: review on literature and an algorithm

The Radon transform is an essential mathematical method in the topic of image reconstruction and deblurring used to analyze and reconstruct images from their projections. Because this tool takes advantage of projections, Radon Transform is regarded as bright method to find blur parameters which mentioned as blur length and blur angle. Its abilities and outputs ensure that blur parameters can be identified from Radon space.

Radon Transform basically, reveals and estimates linear motion blur characteristics via integrating image along defined directions. This transform is expressed as,

$$R(\rho,\theta) = \int_{-\infty}^{\infty}\int_{-\infty}^{\infty}\beta(x,y)\partial(\rho - xcos\theta - ysin\theta)dxdy \qquad (3.2)$$

where $R(\rho,\theta)$ denotes radon transform of a two-dimensional real valued function $\beta(x,y)$, along a line making angle θ with x axis and at a distance ρ from the origin, ∂ is dirac delta function [36].

Most of the applications which is used to estimate PSF function with motion blur parameters, RT is applied on log spectrum of FFT image. As previously discussed, motion angle and pixel length can be seen from frequency spectrum of image that contains uniform linear motion.

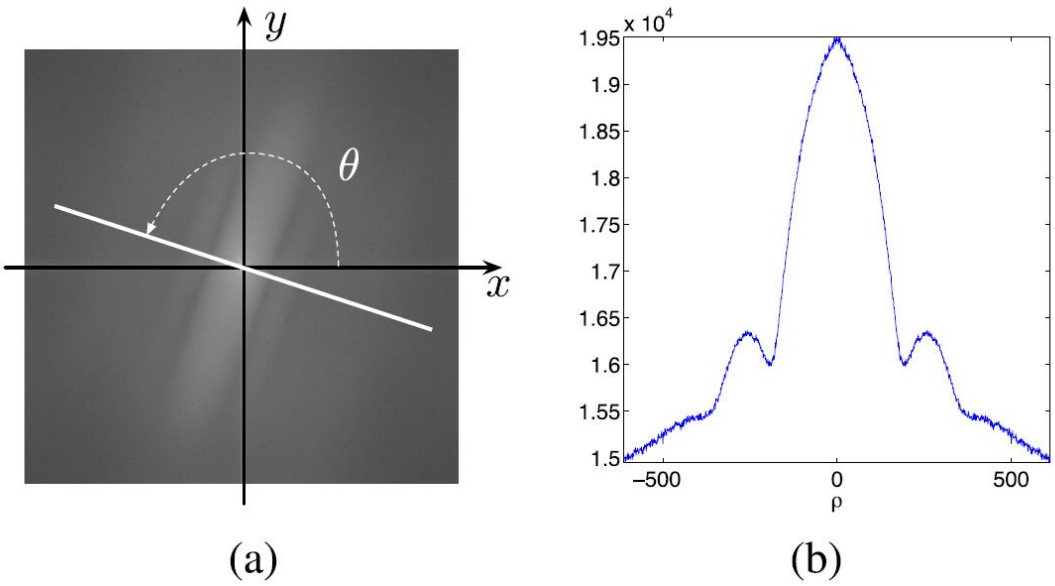

Figure 3.5. (a) Logarithm of the power spectrum of image (white line represents direction of Radon transform) (b) Output of RT (angle θ=155°) [33]

From Figure 3.5 (a), log spectrum of an image can be seen. Also, (b) indicates output of the RT through the white line which makes 155° angle with center. It can be interpreted

that, output of the RT of the log scaled image, bright points are the highest points of RT.

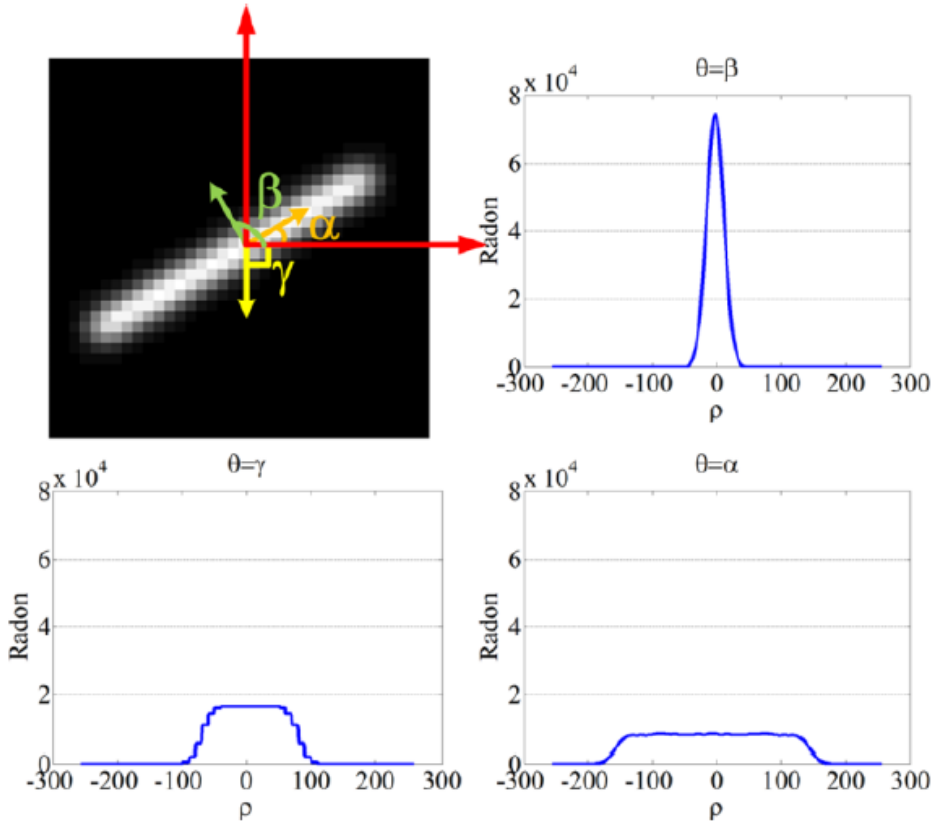

Figure 3.6. Radon transform of an image in three different directions respectively β, γ, α [34]

From Figure 3.6, there are three different angles which is perpendicular to the line in the image, perpendicular to the y axis, and same axis with the line. It can be seen from the output of the Radon transform through the pixels that, highest peak can be obtained from angle β, which is perpendicular to the center lobe of the log spectrum. Also, lowest but longest peak can be derived from the line which is the equivalent to the central lobe angle α through the RT of central lobe [34]. Under these circumstances, if we take RT of an image through angles between $(-\pi, +\pi)$, central maximum points are the motion blur angle parameters of blurred image perpendicular to the central lobe [36], [34]. Blur length in pixels is the division of 1D size to difference between first zero points of the peak point.

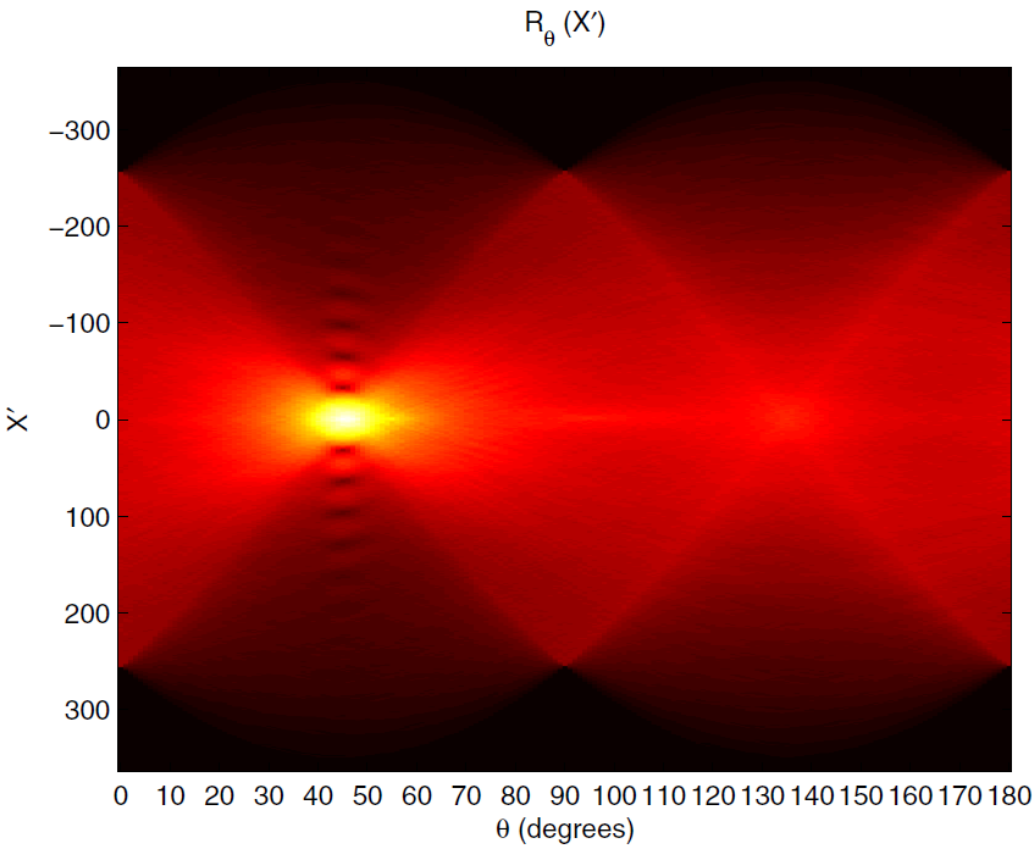

Figure 3.7. RT space of image when L=16 pixels and θ =45° (x: pixels, y degrees) [35]

From Figure 3.7, shows the results of RT when blur length is 16 and blur angle is 45°. Through the X axis, brightest points (between low intensity points) show the effected pixels and from motion blur and through the Y axis, brightest points approximate the blur angle [35].

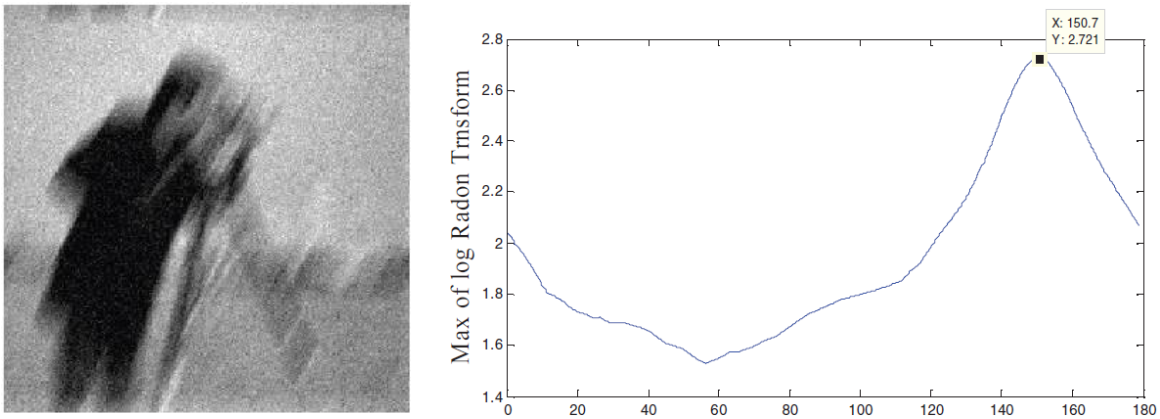

(a) (b)

Figure 3.8. (a) Cameraman image with motion blur L=30 pixel and θ =60° (b) RT of Log spectrum of (a) [36]

In Figure 3.8, RT is applied on cameraman image with 60° blur angle with 30 pixels. From resultant graph, among brightness points through 0° and 180° , minimum point shows the blur angle and brightest point shows the angle perpendicular to the blur angle, which supports previous ideas [36].

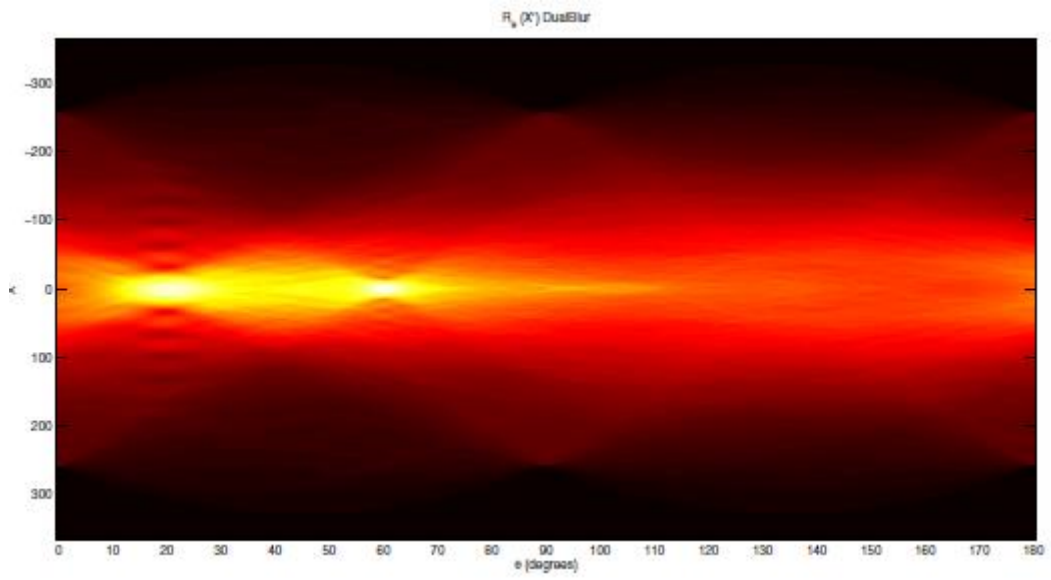

Figure 3.9. RT for spatially variant image for L=16 pixels θ =20° and L=32 pixels and θ=60° [35]

Also, RT can be performed for spatially variant motion blurred images, for example from Figure 3.9, there are two different blur parameters [35]. Also, from Figure 3.9, inverse proportion between blur length and difference between two successive zero points can be seen clearly.

Table 3.2. Algorithm – PSF Estimation with RT and Deconvolution of Blurred Image

1: Convert blurred observed RGB image to gray level image

2: Compute gradient of gray level blurred image ($[\boldsymbol{\nabla g(x,y)}]$)

3: Compute Fourier Transform of gray level image at step 2 ($\boldsymbol{F}[\boldsymbol{\nabla g(x,y)}]$)

4: Calculate log spectrum of FFT gray scale image from step 3 (log ($|\boldsymbol{F}[\boldsymbol{\nabla g(x,y)}]|$))

5: Use Hanning window method to eliminate boundary artifacts

6: Employ low pass filter to eliminate noise and get sinc like structure

7: Apply RT to the output of step 6

8: Find blur angle $\boldsymbol{\theta}$ where output of RT is min

9: Find blur length L in pixels between parallel dark lines from the output of RT

10: Generate PSF function based on the blur parameters from the output of step 8 and step 9

11: Perform deconvolution to the blurred image with PSF from step 10

3.1.3. Cepstrum analysis method: review on literature

Cepstrum analysis is a method used in signal processing to study the periodic patterns within the frequency spectrum of signals. Researchers apply this technique in fields like speech processing, radar signal analysis, seismology, and vibration analysis. The term "cepstrum" was coined by rearranging the first four letters of "spectrum," highlighting the signal transformation aspect.

This method consists of two primary steps. First, researchers compute the power spectrum of a signal. Next, they perform the inverse Fourier transform on the logarithm of the power spectrum. Mathematically, this process can be expressed as follows:

$$C(p,q) = F^{-1}\{1 + log|G(u,v)|\} \tag{3.3}$$

In this equation, G (u, v) is the Fourier Transform of g (x, y), C (p, q) is the cepstrum and F^{-1} is the Inverse Fourier Transform [40]. To avoid negative infinity, "+1" is added to log spectrum [42].

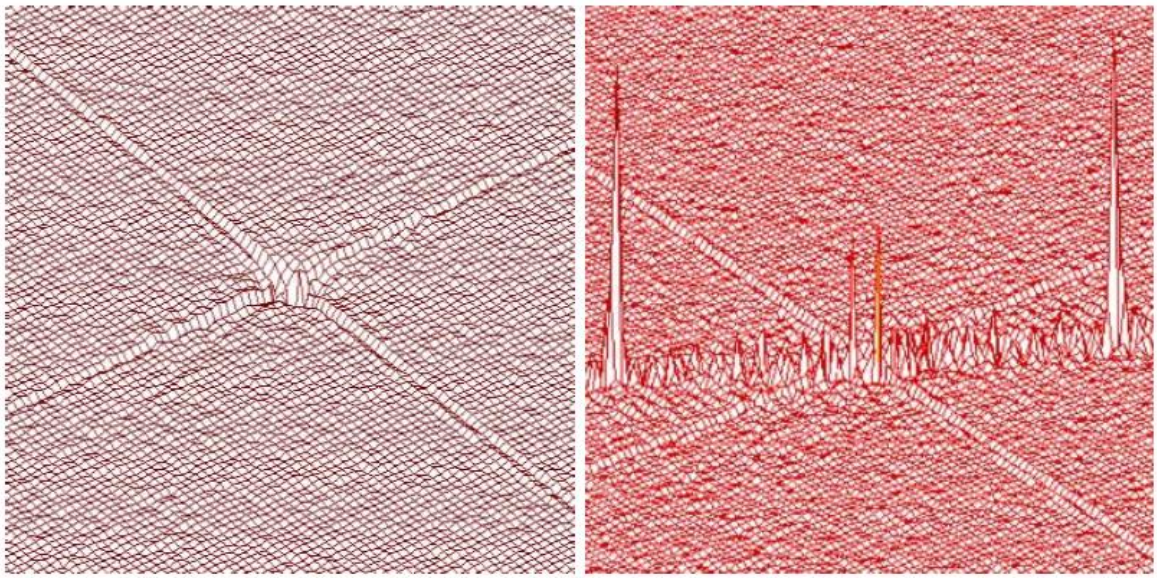

Figure 3.10. (a) Motion blur free image cepstrum, (b) Motion blured image cepstrum with L=30 and θ =30°

In the literature, recent studies on motion deblurring and PSF estimation with cepstrum analysis mostly evaluate RT, HT or frequency domain analysis as better way to find motion angle [40], [41], [42], [43], [44], [45], [48].

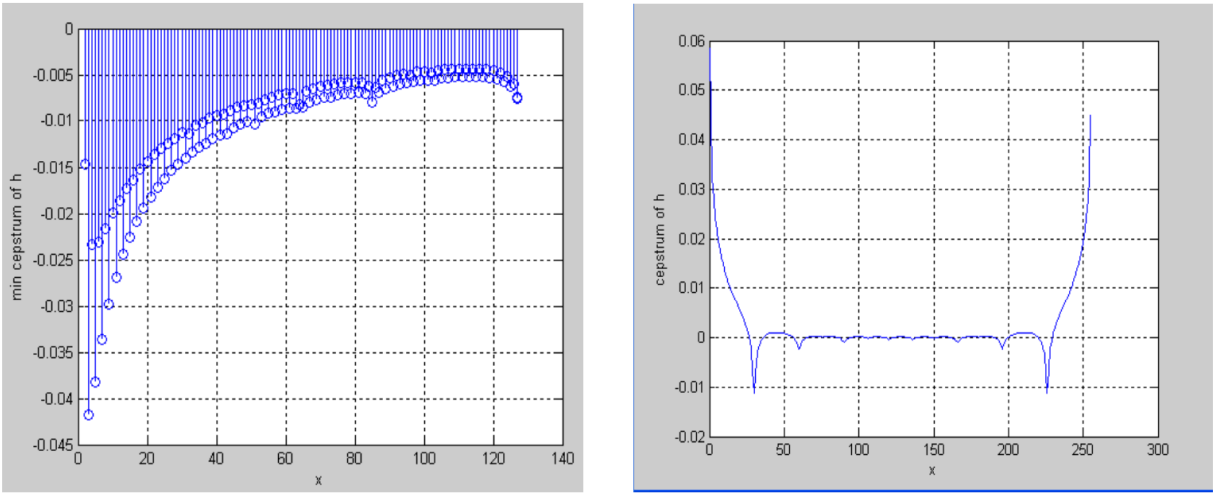

Figure 3.11. Relationship between cepstrum analysis and blur length [43]

According to [43], cepstrum shows minimum at L and N-L-1 along x axis. Which is 30 and 225 in this case.

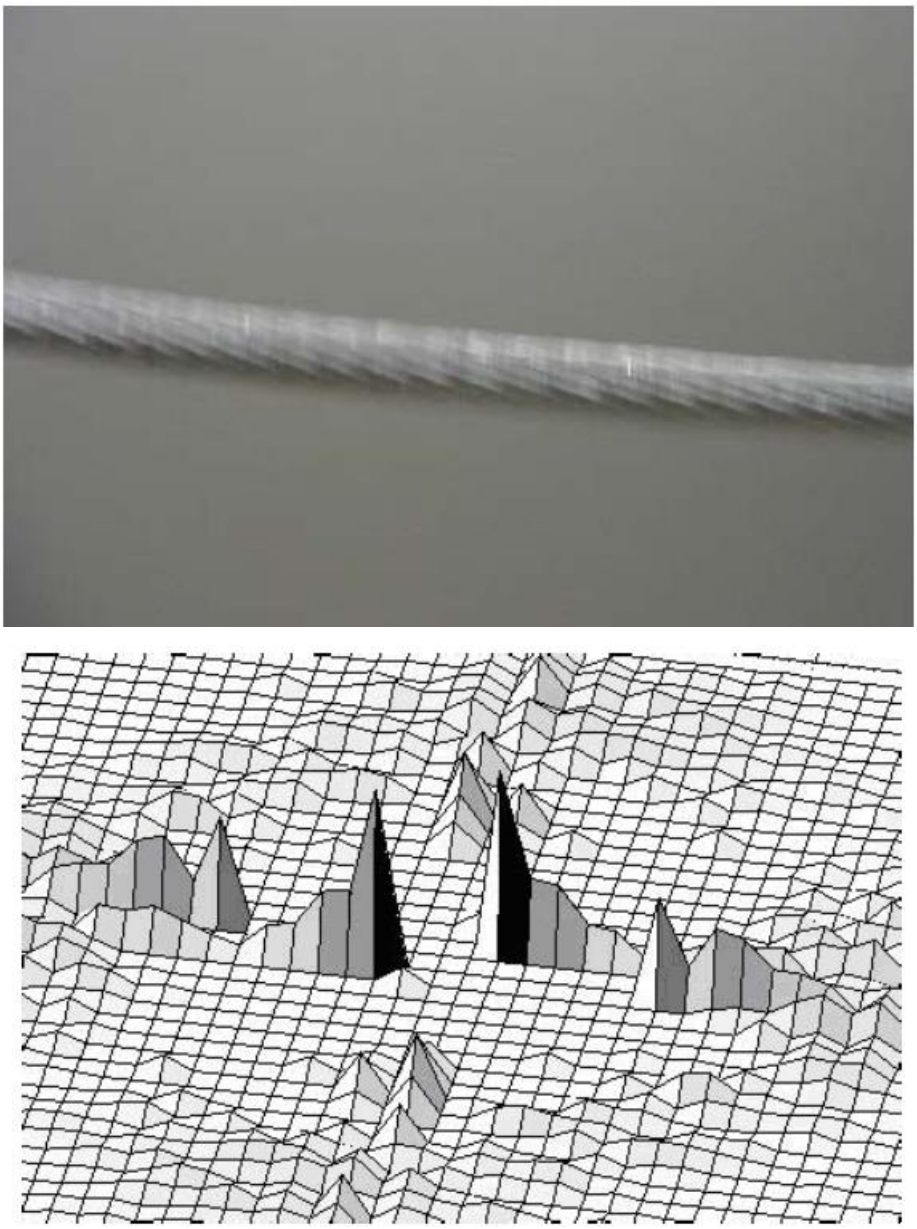

Figure 3.12. Cable image and its cepstrum [48]

According to [42] and [48], difference between minimal points is equal to blur length multiplied by 2.

Table 3.3. Algorithm – PSF Estimation with CA and Deconvolution of Blurred Image

1: Convert blurred observed RGB image to gray level image
2: Compute Fourier Transform of gray level image at step 1
3: Calculate log spectrum of FFT gray scale image from step 2

4: Accomplish binarization of image from step 3

5: Apply low pass filter to the log magnitude spectrum

6: Choose appropriate threshold to identify central lobe

7: Calculate angle of the central lobe this is the blur angle

8: Rotate log magnitude spectrum with respect to calculated angle from step 7

9: Find cepstrum

10: Estimate blur angle L from the cepstrum this is the difference between 2 minimums

11: Generate PSF function based on the blur parameters from the output of step 7 and step 10

12: Perform deconvolution to the blurred image with PSF from step 11

3.2. Purpose

So far, methodologies of linear uniform motion blur PSF estimation methods from frequency spectrum are studied. This research aims to improve image processing by creating a practical method for removing motion blur. The goal is to make theoretical models usable in real-world situations. By achieving this, the study contributes to enhancing digital image restoration techniques, which can be applied in areas like photography, medical imaging, surveillance, and remote sensing. Key point of this study is applying simple and non-iterative method to form PSF in 50ms. This is very fast and easy to apply method with respect to other algorithms.

4. METHOD

In this section, we discuss how we improve blurry images caused by linear uniform motion. We use techniques like Point Spread Function (PSF) estimation and Wiener deconvolution. These methods are based on recent advancements in the field. At the end of this study, algorithm applied to Lenna image then, REDS dataset to check real world potency.

We use the REDS dataset because it contains high-quality images that mimic different types of real-world motion blur. This dataset serves as a reliable platform for testing the effectiveness of our deblurring techniques. Each image in the dataset has synthetic linear motion blur, allowing us to validate the accuracy of PSF estimation and deconvolution methods.

Before we use the deblurring techniques, we first turn the images into grayscale. This makes the calculations easier. Also, we adjust the pixel values by thresholding so that they fall within the range of [0, 1]. This helps ensure consistent processing for all the images.

PSF is like a blueprint for how blur happens in an image. When it comes to linear motion blur, we can think of the PSF as having a specific length and angle. Getting these details right is really important for fixing blurry images.

We estimate the point spread function by analyzing the frequency domain. We use the properties of the Fourier transform and logarithmic transform to identify the characteristics of linear motion.

We use a technique called Wiener deconvolution to fix blurry images. This method is effective because it balances the trade-offs between removing blurriness and avoiding noise amplification.

Table 4.1. Algorithm Blind Image Deblurring of Linear Motion with Simple PSF Estimation in Frequency Domain and Wiener Deconvolution

1: Convert blurred observed RGB image to gray level image
2: Gaussian and Laplacian filter to eliminate noise
3: Compute Fourier Transform of gray level image
4: Calculate log spectrum of FFT gray scale image
5: Apply thresholding to the log magnitude spectrum

6: Choose appropriate threshold to identify central lobe

7: Find brightest pixels at each row

8: Calculate distance from brightest pixels to the origin (row, column)

9: Use arctan to calculate blur angle

10: Rotate LT spectrum by blur angle by keeping row and column size of the original image same

11: Bit plane slice rotated LT spectrum image

12: Use 4th bit plane

13: Make 2D rotated LT spectrum 1D by summing columns

14: Calculate distance between points (right of the peak and left of the peak) that is half size of the peak point

15: Output of step 9 is blur angle and output of step 14 is blur length, form PSF

16: Deconvolve image with wiener method by using output of step 15

The Peak Signal-to-Noise Ratio (PSNR) compares the strength of a signal to the impact of noise. It's a way to assess image quality. This metric will be mostly used to compare images with motion blur and deblurred image. It is calculated as:

$$PSNR = 10 \log_{10} \left(\frac{MAX_I^2}{MSE} \right) \tag{4.1}$$

MSE is the mean squared error between the original and restored images, MAX_I is maximum pixel value of the image [61].

$$MSE = \frac{1}{MN} \sum_{i=1}^{M} \sum_{j=1}^{N} \left(I(i,j) - K(i,j) \right)^2 \tag{4.2}$$

I is original image and *K* is restored image, *i* and *j* states pixelwise operation [61].

5. EXPERIMENTAL RESULTS & DISCUSSION

5.1. Blur Angle Estimation

First milestone of proposed deblurring algorithm is blur angle estimation. To find the blur angle, Lenna image is used as sample image. As it can be seen from image Figure 5.1, uniform motion blur can be applied to input image by defining PSF parameters.

(a) (b)

Figure 5.1. (a) Sample Lenna image (b) Motion blurred Lenna image with θ =60° L=30 pixels

To extract blur direction parameter, we should take FT of image. Taking only FT does not work, it is vital that we should make uniform blur parameters visual. To accomplish this, LT is applied to image.

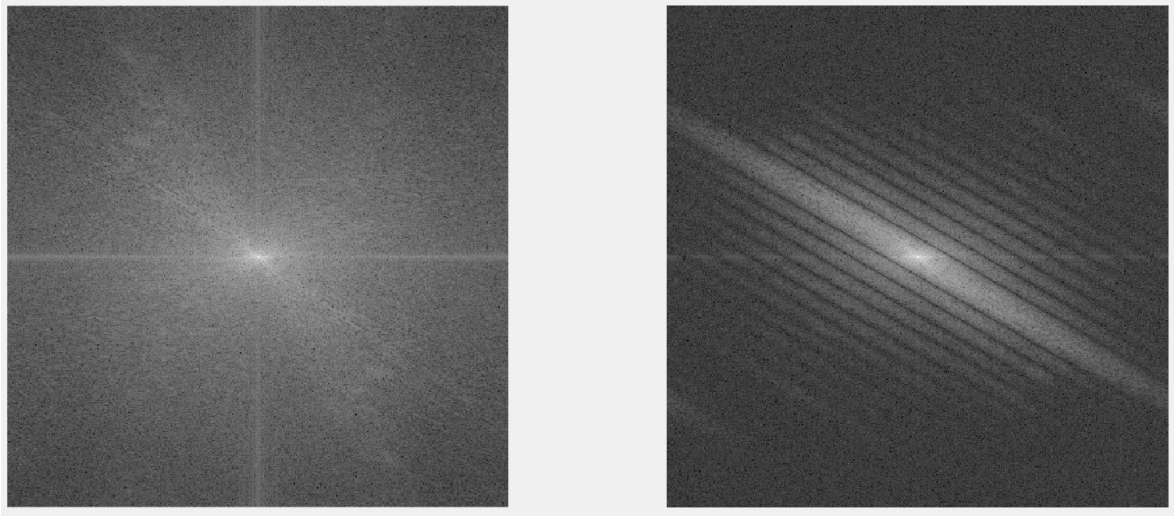

(a) (b)

Figure 5.2. (a) LT of original Lenna image (b) LT of motion blurred image with θ =60° L=30 pixels

Thresholding should be applied to image to make blur patterns more visible and distinguishable.

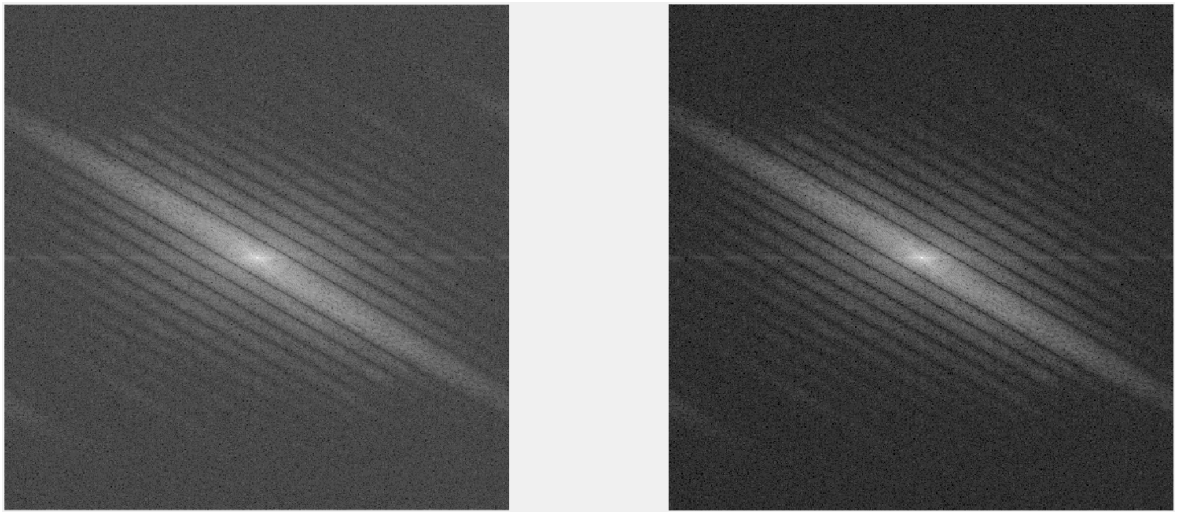

(a) (b)

Figure 5.3. (a) LT spectrum of motion blurred image (b) Thresholded LT spectrum of motion blurred image

A Monte-Carlo analysis was performed to find the thresholding value at which we obtained the best results while keeping the other parameters constant. As a result of the analysis, choosing the relevant value as 3 provided the best results for our data set. The boundary values selected for Monte-Carlo analysis are between 2-15.

To find the angle, first find the maximum pixel value in each row of the upper half of the input LT image. Then calculate the inclination angle of maximum pixel values from the origin of the coordinate system. The inclination angle (β) is calculated according to equation below [28]. θ is the blur angle.

$$\beta = tan^{-1}\left(\frac{d_y}{d_x}\right) \tag{4.3}$$

Calculate inclination angle values for every maximum pixel point.

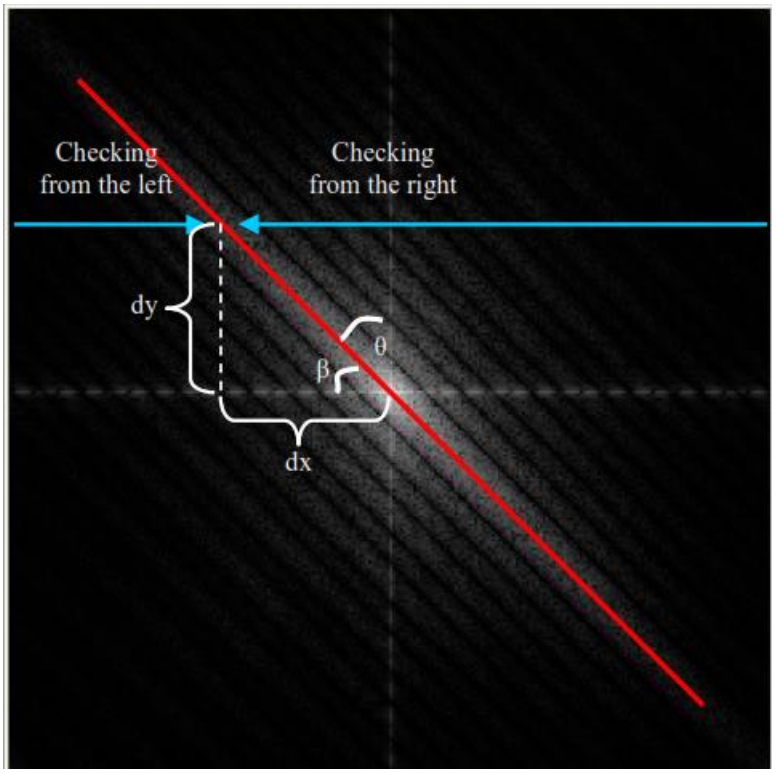

Figure 5.4. Calculations to blur angle [28]

Table 5.1. Angle estimation results on Lenna image for θ = [+90°- -90°] when L=30 pixels

Image	Degrees	Number of Errors (5°) (True)	Number of Estimated Degrees (False)	Estimation %	Errors %
Lenna (L=30 pixels)	[-90° – +90°]	11	170	%93,92	%6.07
Lenna (L=15 pixels)	[-90° – +90°]	37	144	%79,55	%20,44

30 pixels motion length Lenna image is tested for θ = [+90°, -90°] angles. Estimated results are categorized as true when difference between blur angle and estimated blur angle is 5°. Estimated results are categorized as false when difference between blur angle and estimated blur angle is larger than 5 °. As seen from **Hata! Başvuru kaynağı bulunamadı.**Table 5.1, increase in blur length, increase the accuracy of estimated blur angle.

Angle estimation is most critical part of this algorithm, because finding blur length parameter is depends on the rotation of LT space by estimated angle.

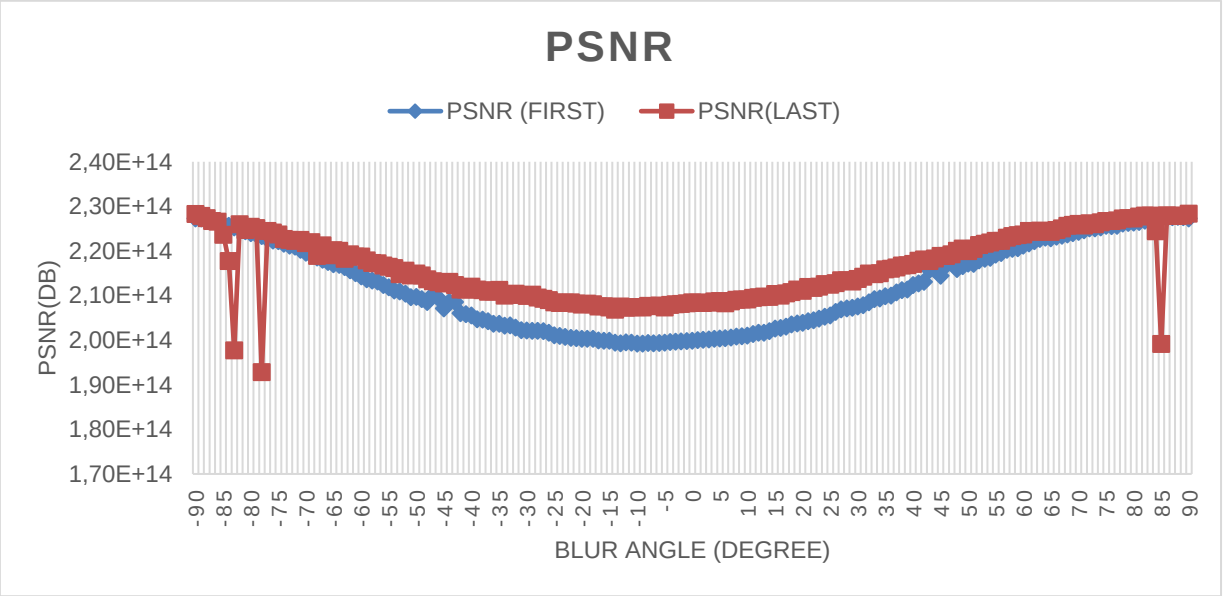

Figure 5.5. PSNR of motion blurred(blue) and deblurred image(red) between θ = [-90°, +90°] when L=30 pixels

Figure 5.5 shows the PSNR values of motion blurred(blue) and deblurred(red) images. Wiener deconvolution method applied to blurred image. PSNR(FIRST) is the PSNR of blurred image to original image, PSNR(LAST) is the PSNR of deblurred image by PSF of estimated angles to original image. PSNR of deblurred image is mostly higher from blurred image.

5.2. Blur Length Estimation

To estimate blur length, LT spectrum of image should be rotated by estimated blur angle. It would be wise to keep size of the image same to make calculations easy and coherent. From Figure 5.6, LT spectrum and rotated spectrum of motion blurred image is shown.

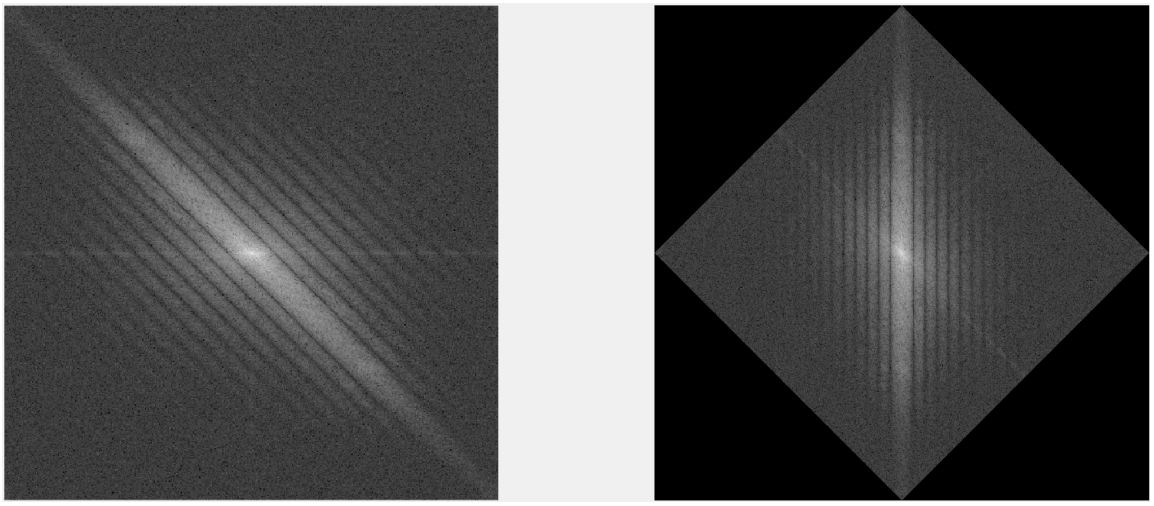

(a) (b)

Figure 5.6(a) LT spectrum of motion blurred image (b) LT spectrum of rotated image with estimated angle parameter

There is a relation between blur length and size of the main lobe in LT domain. Figure 5.8 shows the relation between size of the blur length and size of the main lobe, that is inversely proportional (uniform motion blurred image with θ=0°, L=10 pixels and L=40 pixels). When calculating blur length, we should make 2D image 1D (sum the columns). Half-length of the main lobe gives the length parameter.

$$L = \frac{2L_0}{d} \tag{4.4}$$

L_0 defines the row size of the image, d is main lobe width and d is the amount of the blur length [27]. This calculation is affected by the noise. Bit plane slicing method is needed to get noise-free image to calculate length of the blur accurately, which is a better way than filtering to eliminate noise. Rotated image is uint8 image which means there is 8 different bit planes.

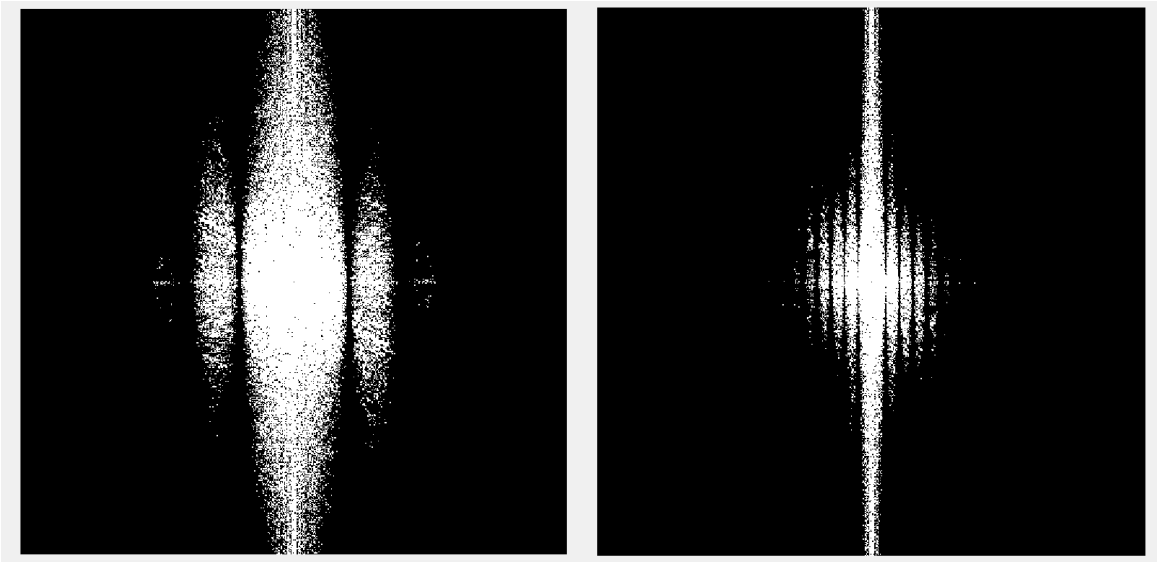

(a) (b)

Figure 5.7. (a) L=10 pixels (b) L=40 pixels

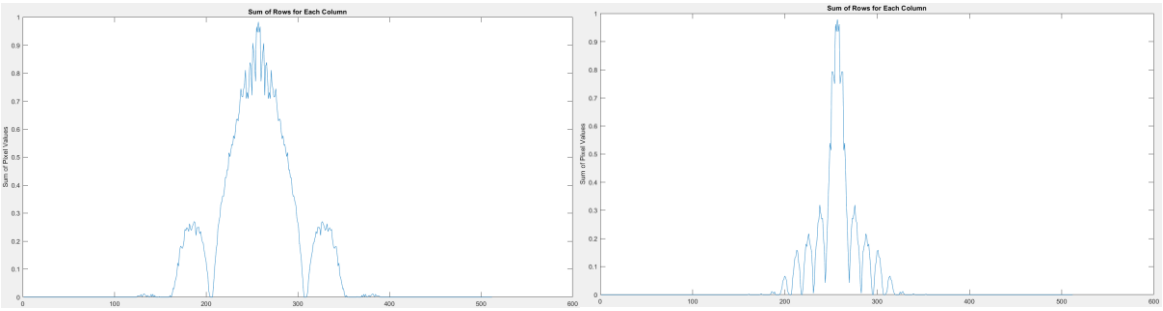

(a) (b)

Figure 5.8. (a) L=10 pixels (b) L=40 pixels

From Figure 5.9, bit plane 4 gives the clearest (between bit planes of rotated spectrum) 2D matrix to calculate width of the main lobe.

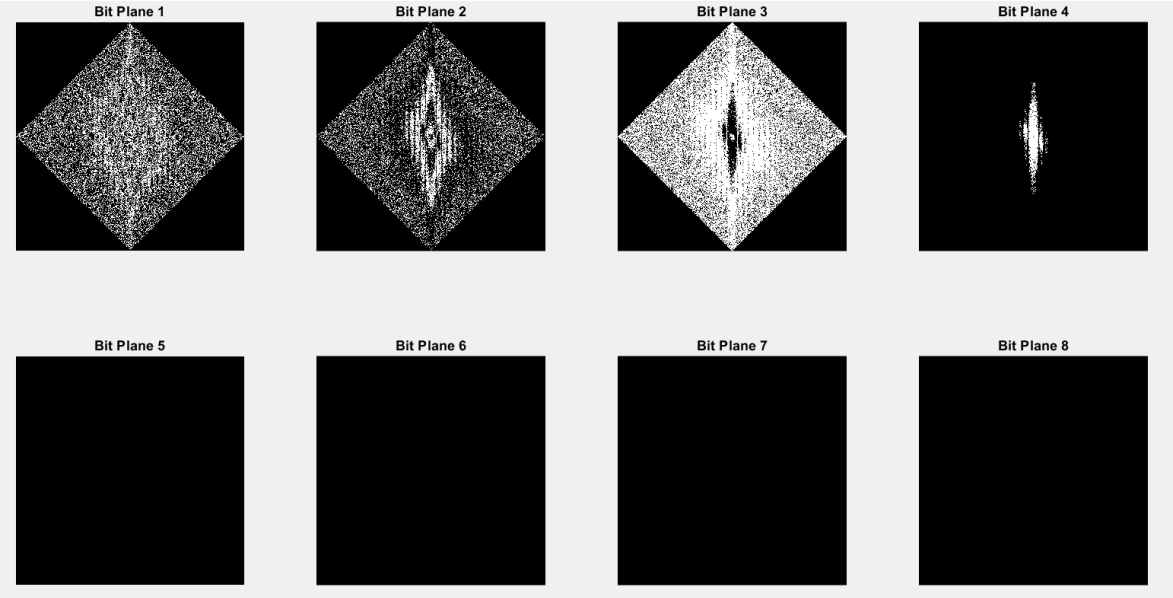

Figure 5.9. Bit planes of rotated LT spectrum L=30 pixels

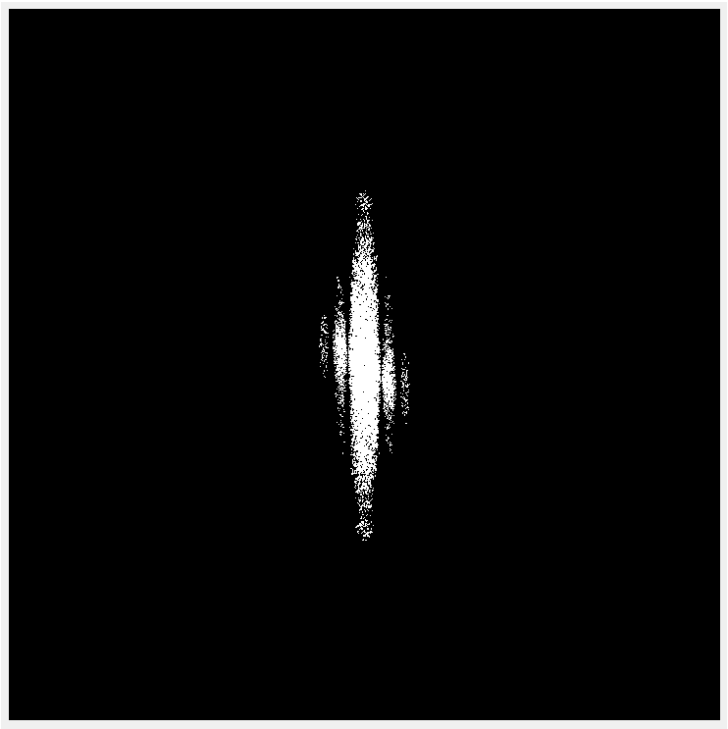

Figure 5.10. 4th bit plane of rotated LT spectrum L=30 pixels

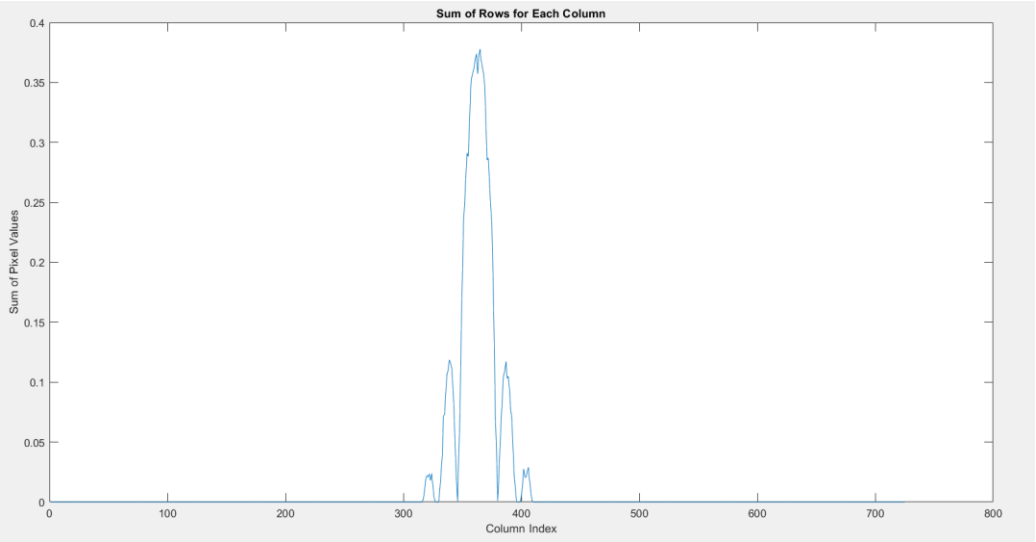

Figure 5.11. 1D image L=30 pixels

Peak point of the graphic corresponds to the centre of the main lobe. We should find the first zeros closest to the peak point from right and left. For better approximation, difference between half size of the peak point should be calculated. Result of this step, gives the blur length.

45° motion angle Lenna image is tested for L = [10 40] angles. Estimated results are categorized as true when difference between blur length and estimated blur length is 5. Estimated results are evaluated as false when difference between blur angle and estimated blur angle is larger than 5 pixels when L= [10 - 40] and 1 pixel when L= [1 - 10] (because 5 pixels error rate is high for L= [1 - 10] pixels).

Table 5.2 Length estimation results blur angle θ=45°, L= [10 - 40] and L= [0 - 10]

Image	Lengths	Number of Errors (True)	Number of Estimated Lengths (False)	Estimation %	Errors %
Lenna	[10 - 40]	0 (5 pixels)	31 (5 pixels)	%100	%0
Lenna (with different threshold)	[1 - 10]	0 (1 pixels)	10 (1 pixels)	%100	%0

Figure 5.5 shows the PSNR values of motion blurred(blue) and deblurred(red) images. PSNR(FIRST) is the PSNR of blurred image to original image, PSNR(LAST) is the PSNR of deblurred image by PSF of estimated blur lengths to original image. Wiener

deconvolution method applied to blurred image. PSNR of deblurred image is mostly higher from blurred image.

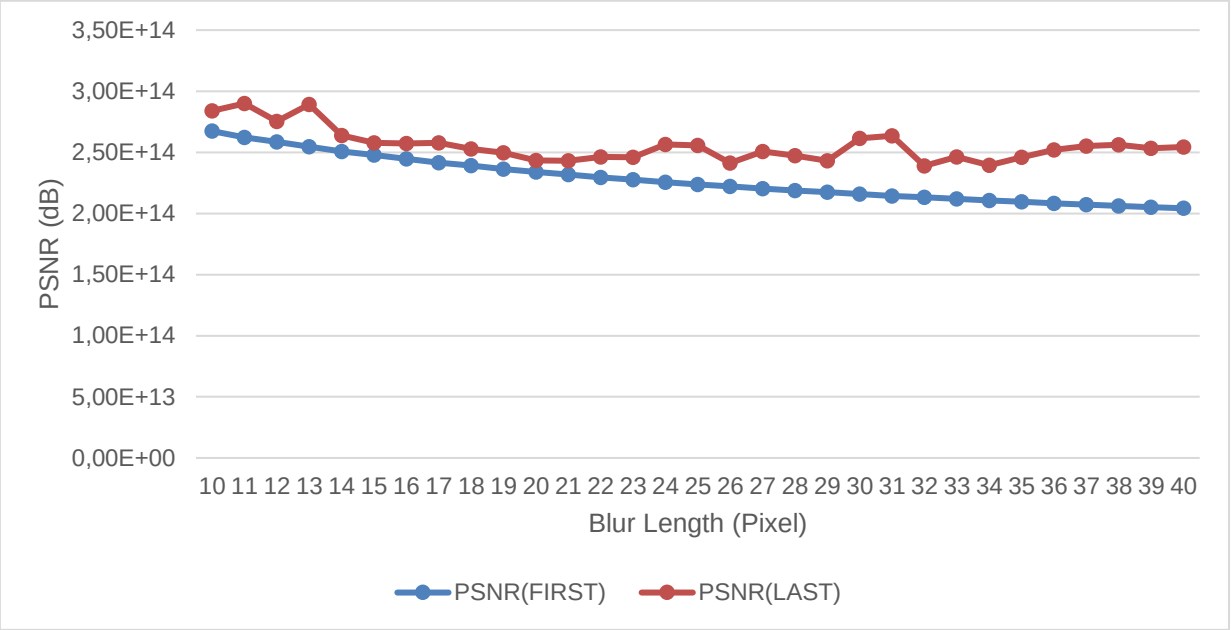

Figure 5.12. PSNR of blurred(blue) and deblurred image(red)

5.3. Wiener Deconvolution

Figure 5.13 shows blurred and restored Lenna image. Wiener deconvolution is applied to blurred image by using estimated blur parameters from previous steps.

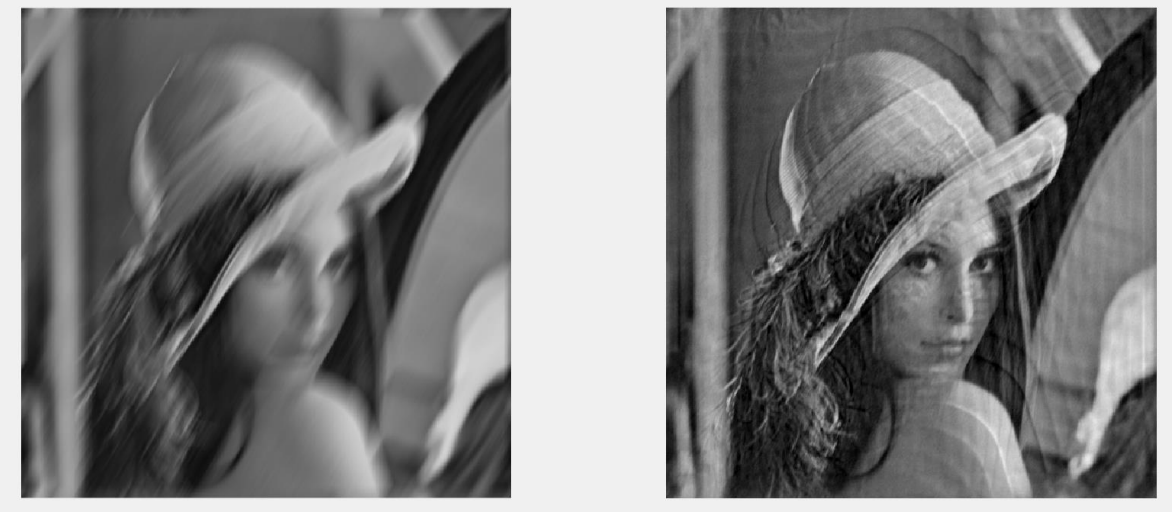

(a) (b)

Figure 5.13. (a) Blurred (b)Restored Lena Image

Ringing artifacts frequently arise during image deblurring as in Figure 5.13 (b). These artifacts manifest as oscillatory patterns surrounding sharp edges and can substantially impact the perceived fidelity of the deblurred image.

When an image undergoes blurring, its high-frequency components—those associated with sharp edges and fine details—are attenuated. During the deblurring process, particularly when using methods like Wiener deconvolution, these high-frequency components are amplified to restore sharpness. However, this amplification can also accentuate any pre-existing noise in the image, resulting in undesirable ringing artifacts [63].

In the context of image blurring, the suppression of high-frequency components—those associated with sharp edges and fine details—occurs. Subsequently, during the deblurring procedure, particularly when employing methods such as Wiener deconvolution, these high-frequency components undergo amplification to restore sharpness. However, this amplification can inadvertently accentuate pre-existing noise within the image, resulting in the emergence of undesirable ringing artifacts [63].

The PSF characterizes the spatial distribution of light from a single point source as it disperses within an image due to blurring. When the estimated PSF lacks precision, the deblurring algorithm may fail to accurately reverse the blur, leading to undesirable artifacts. Even minor deviations in the PSF can result in conspicuous ringing, as the algorithm attempts to compensate for an erroneous blur model.

In the context of deconvolution, the image boundaries present a challenge. Algorithms typically operate under the assumption of infinite image extension, but the artificial edges at the boundaries introduce discontinuities. These discontinuities give rise to ringing artifacts in the resulting deblurred image.

Deconvolution algorithms, such as Wiener filtering, hinge upon specific assumptions regarding noise and blur properties. However, real-world images frequently deviate from these assumptions, leading to imperfect deconvolution and the emergence of ringing artifacts. Notably, deviations from white noise characteristics or inaccuracies in modeling the blur kernel can contribute to the production of such artifacts.

In the context of deconvolution, regularization methods serve to stabilize solutions and mitigate noise amplification. However, inadequate tuning of regularization parameters can lead to undesirable outcomes: overly aggressive regularization may suppress fine details along with noise, while overly lenient regularization can permit the persistence of ringing artifacts.

5.4. Application on REDS Dataset

In this section, we present the experimental results of our blind image deblurring approach on the REDS dataset. We implemented our deblurring algorithm using MATLAB. The experiments were conducted on a subset of the REDS dataset, which includes images with varying degrees of linear motion blur. To quantitatively evaluate the performance of our deblurring algorithm, we used the following metrics:

Peak Signal-to-Noise Ratio (PSNR): Measures the ratio between the maximum possible power of a signal and the power of corrupting noise that affects the fidelity of its representation.

Structural Similarity Index (SSIM): Assesses the similarity between the original and deblurred images, considering changes in luminance, contrast, and structure.

Mean Squared Error (MSE): A common metric used in image processing to quantify the difference between two images. It is calculated by averaging the squares of the pixel intensity differences between the original image and the processed image.

The accuracy of our PSF estimation method was validated by comparing the estimated PSF parameters with the ground truth provided in the REDS dataset. The results demonstrated high accuracy, with minimal deviation from the true values. Table 5.3 presents the comparative analysis of the estimated and actual PSF parameters. Mean PSNR between blur and train images is 26.16, mean MSE is 254,07 and mean SSIM is 0.77. From figure below, detailed results for PSNR, MSE and SSIM can be seen.

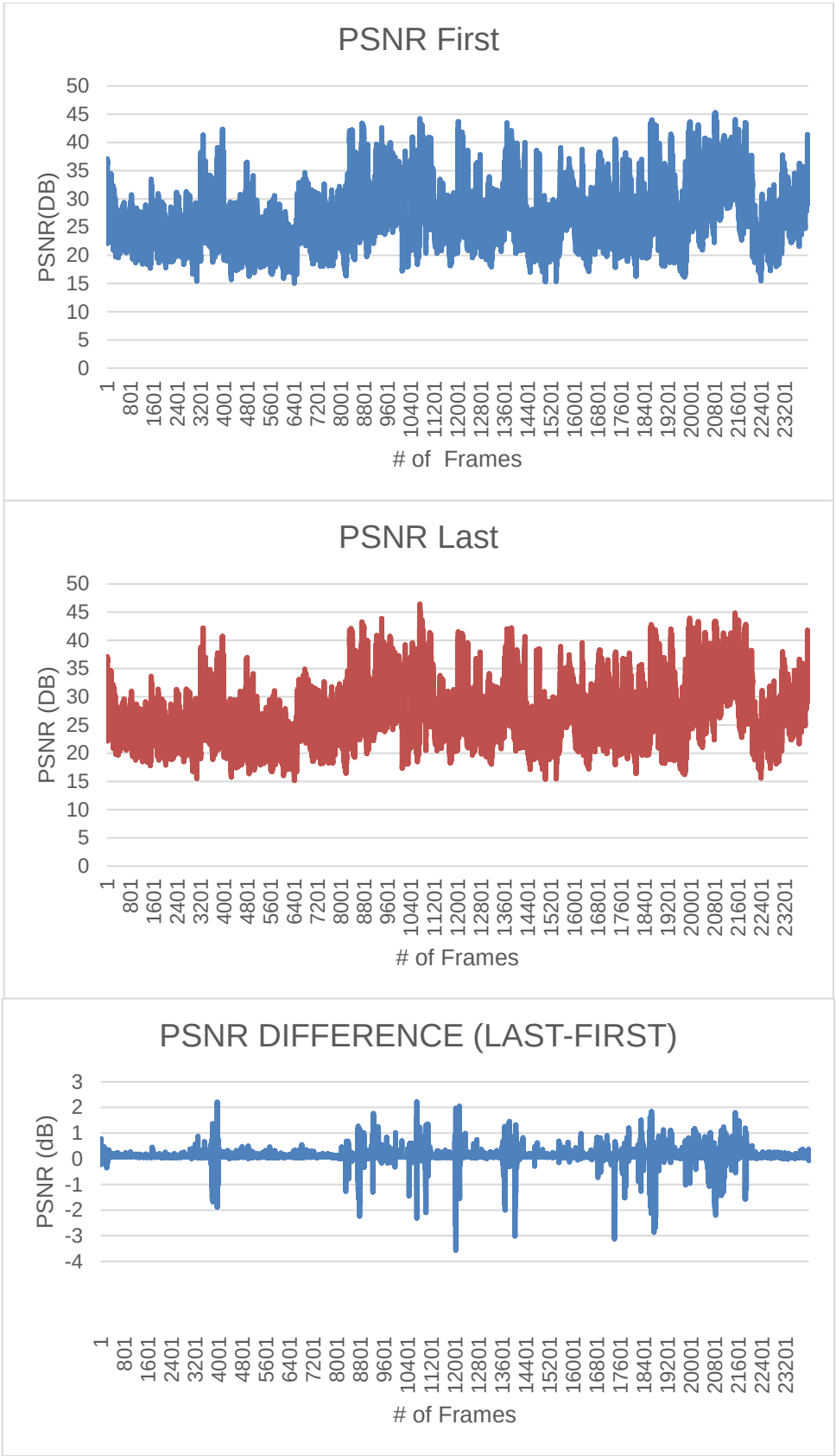

Figure 5.14 PSNR Results of Proposed Algorithm vs Number of Images

Table 5.3 PSNR Comparison

Method/ Algorithm	Mean PSNR Value	SSIM	MSE	Time
Deblur GAN [66]	24.09	0.96	-	850ms
Proposed Algorithm	26.29	0.77	254.07	44ms
EDVR Deblur [65]	34.80	0.88	-	-
VRT [64]	36.79	0.88	-	236ms

PSNR(FIRST) is the PSNR of blurred image to original image, PSNR(LAST) is the PSNR of deblurred image by PSF of estimated blur lengths and angles to original image. PSNR Difference is the difference between PSNR of blurry and deblurred image to sharp image. Wiener Proposed algorithm is faster than iterative and deep learning-based algorithms. Also, it has low computational complexity. At the table, (-) means that there is no information. On the other hand, for real-world scenarios, this algorithm cannot show best results according to PSNR, MSE and SSIM. This method is successful on images which blur angle and length is higher, blur distribution is linear and uniform.

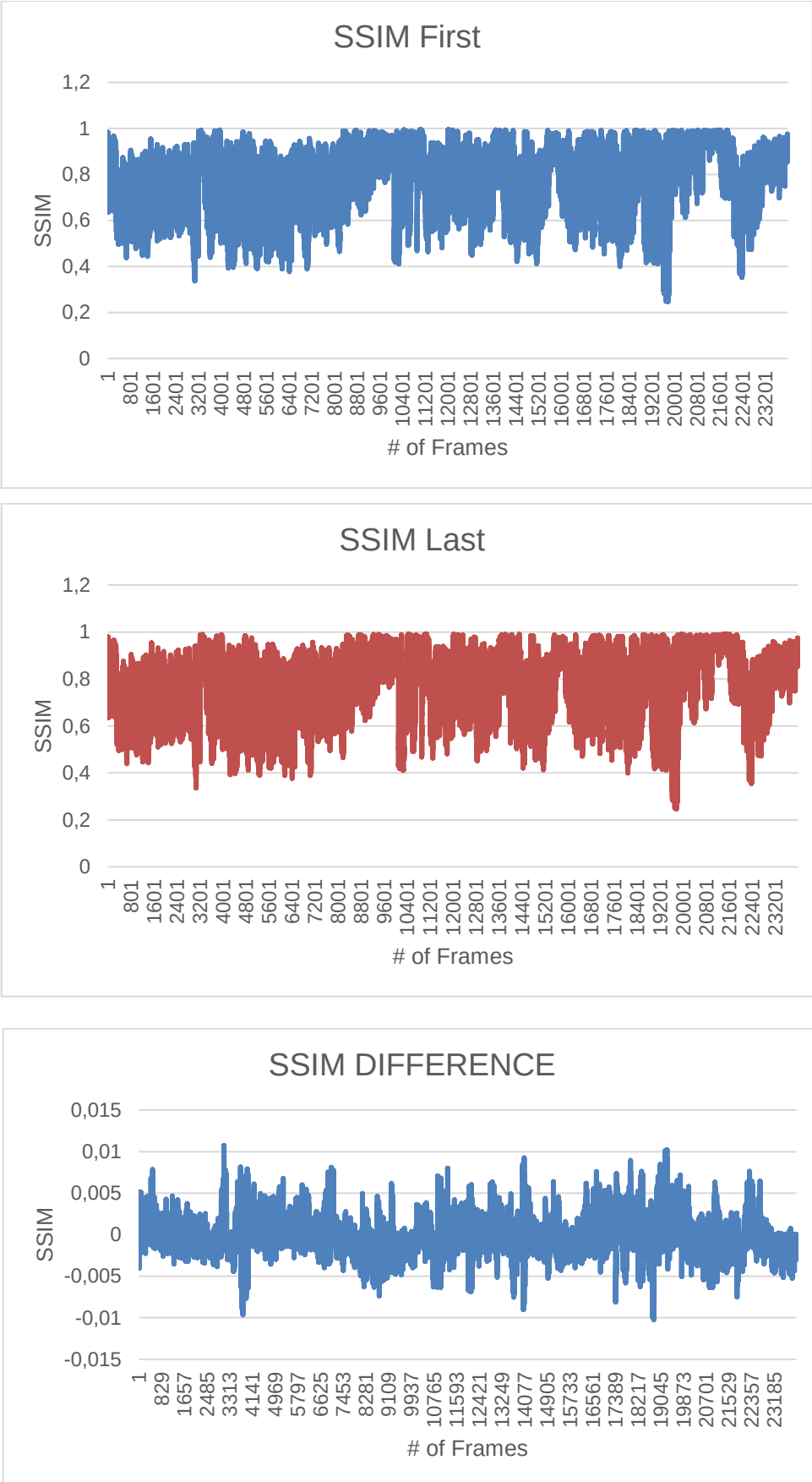

Figure 5.15 SSIM Results vs Number of Images

SSIM(FIRST) is the SSIM of blurred image to original image, SSIM(LAST) is the SSIM of deblurred image by PSF of estimated blur lengths and angles to original image. SSIM Difference is the difference between SSIM of blurry and deblurred image.

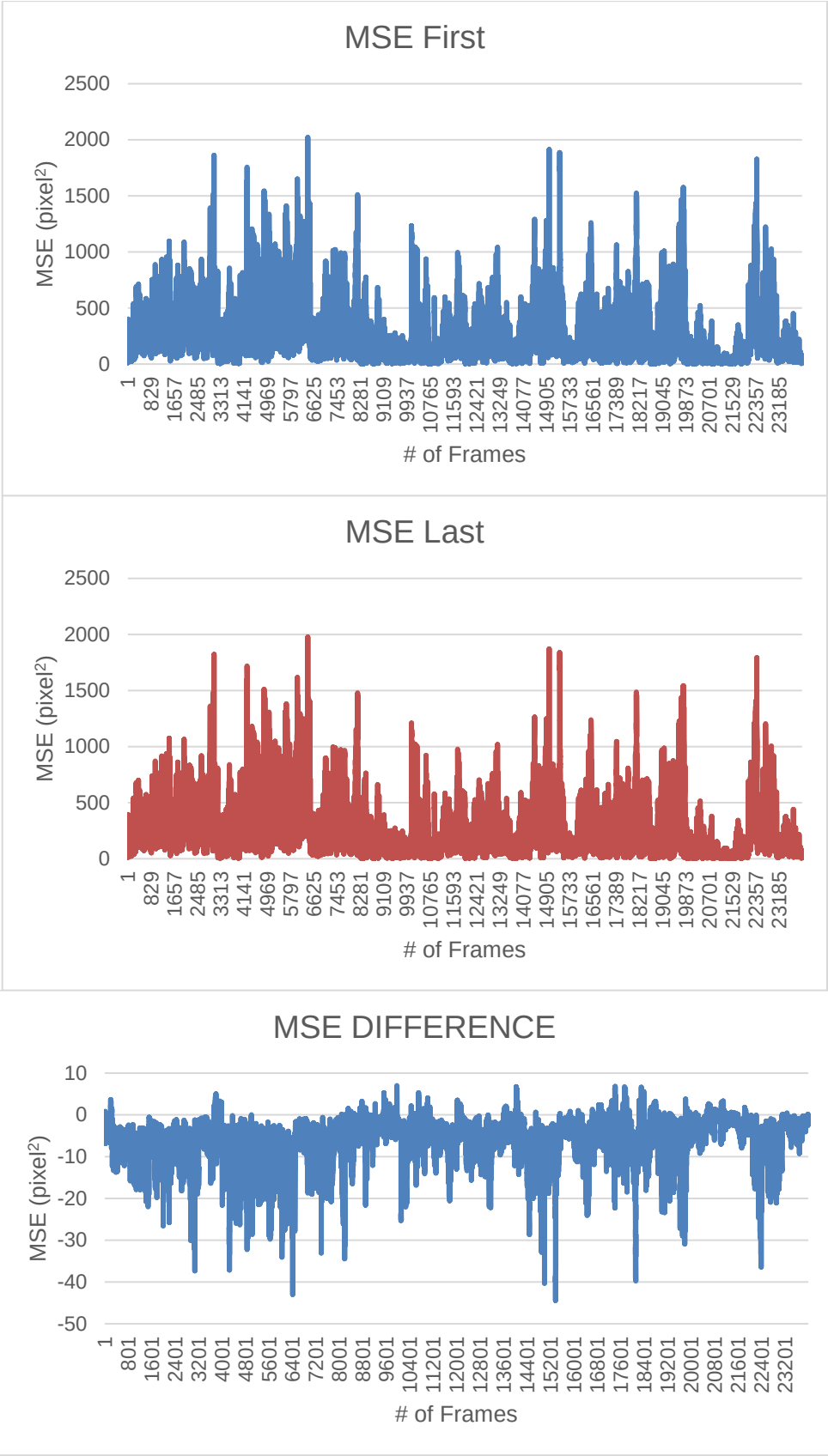

Figure 5.16 MSE Results vs Number of Images

MSE(FIRST) is the MSE of blurred image to original image, MSE(LAST) is the MSE of deblurred image by PSF of estimated blur lengths and angles to original image. MSE Difference is the difference between MSE of blurry and deblurred image.

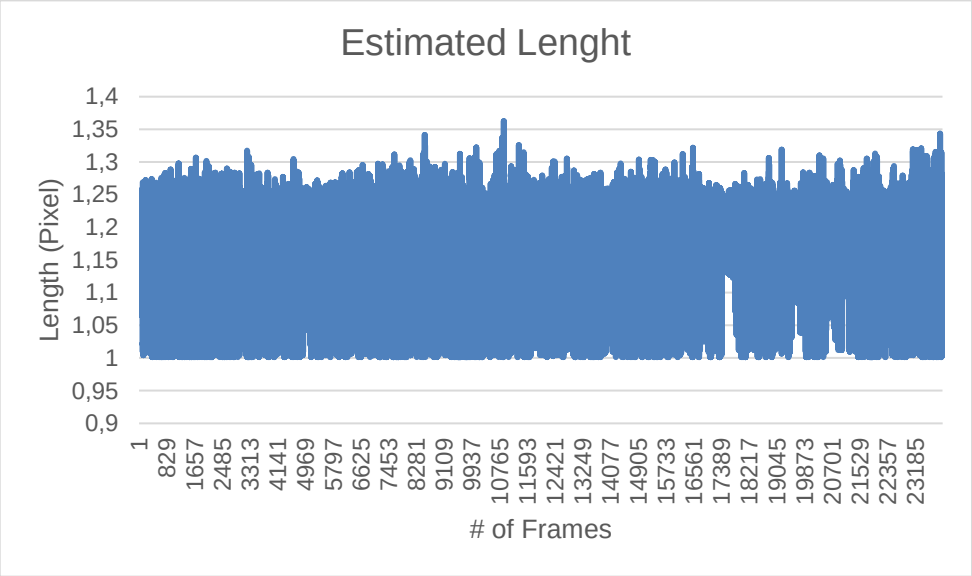

Figure 5.17 Estimated Length vs Number of Images

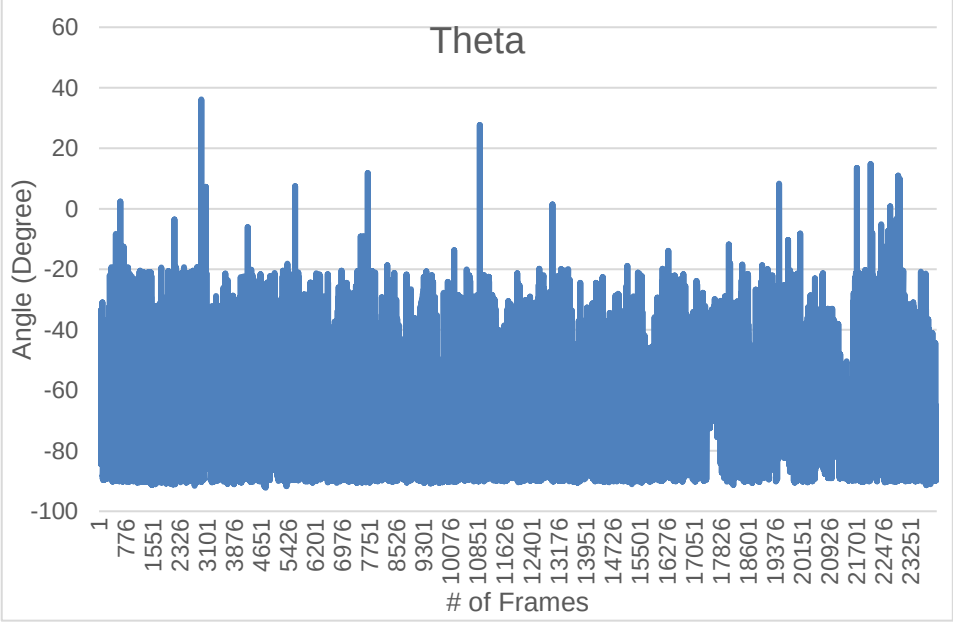

Figure 5.18 Estimated Theta vs Number of Images

6. CONCLUSION AND FUTURE WORK

6.1. Conclusion

In this thesis, we have conducted an in-depth investigation into the challenge of blind image deblurring, with a particular focus on linear uniform motion blur. Our methodology employed straightforward Point Spread Function (PSF) estimation techniques within the frequency domain, coupled with Wiener deconvolution for the image restoration process. This approach draws inspiration from and builds upon the foundational techniques outlined in the seminal works "A Simple PSF Parameters Estimation Method for the De-blurring of Linear Motion Blurred Images Using Wiener Filter in OpenCV" and "Blind Image Restoration with Horizontal Motion Blur Based on Point Spread Function Estimation in Frequency Domain."

Through comprehensive experimentation utilizing the Lena image and REDS dataset, our findings demonstrated a marked enhancement in image quality following the deblurring process. Objective performance evaluation of our deblurring algorithm was conducted using quantitative metrics, specifically Peak Signal-to-Noise Ratio (PSNR), Mean Square Error (MSE) and Structural Similarity Index (SSIM). Furthermore, visual assessments substantiated the efficacy of our approach, revealing significant restoration of fine details and an overall increase in image sharpness.

Our in-depth theoretical discussions on the concept of the Point Spread Function (PSF) and its mathematical representation offered a thorough understanding of the mechanisms underlying motion blur and its mitigation. This foundational knowledge was essential for the development of an effective and robust deblurring algorithm.

Despite the encouraging results, our method is not without limitations. The precision of the PSF estimation is paramount to the mostly level of noise, noise type and success of the deblurring process. Inaccurate PSF estimation can result in suboptimal restoration, especially angle estimation is vital since blur angle is a step for blur length calculation, introducing artifacts and diminishing image quality. This algorithm does not have an important recovery on REDS dataset, because there is different amount and type of noise on images. But it is very fast, compared to other frequency domain or deep learning algorithms.

6.2. Future Work

Several promising avenues for future research could further enhance and extend the findings of this thesis. One of the primary areas for future research is the development of more robust and adaptive PSF estimation methods. Current techniques can be prone to inaccuracies, particularly in scenarios involving different kind and level of noise, complex motion. Machine learning-based approaches, particularly those leveraging deep learning, have demonstrated significant potential in this domain. These methods could enhance PSF estimation accuracy and decrease computation time by giving initial estimation with fast frequency domain analysis and learning from extensive datasets of blurred and sharp image pairs, thereby improving overall deblurring performance.

Another crucial area for future research is the optimization of the computational efficiency of the deblurring algorithm. Real-time applications necessitate rapid processing, which is currently impeded by the computational demands of Wiener deconvolution. Future work could investigate parallel processing techniques, such as utilizing multi-core CPUs or GPU acceleration, to significantly reduce processing times and make real-time deblurring feasible.

While our research primarily addressed linear, uniform motion blur, real-world scenarios frequently involve more complex types of blur, such as rotational, non-linear motion blur, and defocus blur. Extending our methodologies to accommodate these more intricate blur types would yield a more comprehensive deblurring solution. This could entail developing hybrid models that integrate various deblurring techniques or adapting our existing models to address these more complex scenarios.

Integrating the deblurring algorithm with other image enhancement techniques, such as noise reduction, contrast adjustment, and edge enhancement, could further enhance overall image quality. This comprehensive approach could result in a more holistic image restoration process, simultaneously addressing multiple image degradation factors.

Incorporating user feedback or interactive elements to refine PSF estimation and deblurring parameters could significantly enhance the practical usability of the system. User-assisted deblurring could be particularly valuable in professional applications such as medical imaging, surveillance, and forensic analysis, where expert input can guide the deblurring process to achieve optimal results.

To rigorously assess the robustness and efficacy of our deblurring algorithm on uniform motion blurred images, it is imperative to evaluate it across a more extensive array

of datasets. These datasets should encompass images exhibiting varying degrees of noise, diverse types of motion blur, and a wide range of real-world conditions. Such a comprehensive evaluation would yield a more profound understanding of the algorithm's strengths and limitations.

The development of intuitive user interfaces and advanced visualization tools can significantly enhance the accessibility of the deblurring algorithm for non-expert users. These tools can offer real-time feedback, enabling users to observe the effects of various parameter adjustments and gain a deeper understanding of the deblurring process.

Investigating the applications of the deblurring algorithm across various domains, including astronomy, microscopy, and security, can unveil new research opportunities. Each of these fields poses distinct challenges and requirements, and tailoring the deblurring techniques to address these specific needs can foster innovative solutions and advancements.

By addressing these areas, future research can further advance the field of blind image deblurring, enhancing its versatility, efficiency, and applicability across a wider spectrum of real-world scenarios. The ongoing development and refinement of these techniques will ultimately lead to more accurate and reliable image restoration, thereby improving the quality and utility of images in various applications.

REFERENCES

[1] Zhang, K., Ren, W., Luo, W. et al. “Deep Image Deblurring: A Survey,” *International Journal of Computer Vision*, vol. 130, 2103–2130 (2022). doi.org/10.1007/s11263-022-01633-5.

[2] Li, Chumiao. “A Survey on Image Deblurring,” *ArXiv*, 2022, abs/2202.07456.

[3] L. Gondara, "Medical Image Denoising Using Convolutional Denoising Autoencoders," *2016 IEEE 16th International Conference on Data Mining Workshops (ICDMW)*, Barcelona, Spain, 2016, pp. 241-246, doi:10.1109/ICDMW.2016.0041.

[4] D. Kheni, T. Italiya, D. Isarani and D. Karthick, "A novel blind approach for image restoration using adaptive kurtosis-based deconvolution," *2017 2nd IEEE International Conference on Recent Trends in Electronics, Information & Communication Technology (RTEICT)*, Bangalore, India, 2017, pp. 957-962, doi:10.1109/RTEICT.2017.8256740.

[5] C. Thorpe, F. Li, Z. Li, Z. Yu, D. Saunders and J. Yu, "A Coprime Blur Scheme for Data Security in Video Surveillance," in *IEEE Transactions on Pattern Analysis and Machine Intelligence*, vol. 35, no. 12, pp. 3066-3072, Dec. 2013, doi:10.1109/TPAMI.2013.161.

[6] W. Manwei, Z. Fuzhen, Z. Bing and B. Yuyang, "An improved remote sensing image blind deblurring algorithm," *3rd International Conference on Electronic Information Technology and Computer Engineering (EITCE)*, Xiamen, China, 2019, pp. 667-670, doi:10.1109/EITCE47263.2019.9094971.

[7] Fergus, R., Singh, B., Hertzmann, A., Roweis, S. T., & Freeman, W. T. “Removing Camera Shake from a Single Photograph,” *ACM Transactions on Graphics (TOG)*, (2006), 25(3), 787-794.doi:10.1145/1141911.1141956.

[8] M. E. Moghaddam, "A Mathematical Model to Estimate Out of Focus Blur," *2007 5th International Symposium on Image and Signal Processing and Analysis*, Istanbul, Turkey, 2007, pp. 278-281, doi:10.1109/ISPA.2007.4383705.

[9] Y. Liu, G. Zhai, X. Liu and D. Zhao, "Quality assessment for out-of-focus blurred images," *Visual Communications and Image Processing (VCIP)*, Singapore, 2015, pp. 1-4, doi:10.1109/VCIP.2015.7457858.

[10] Lagendijk, R.L., & Biemond, J. "Basic Methods for Image Restoration and Identification," (2009), doi:10.1016/B978-0-12-374457-9.00014-7.

[11] X. Zhu and P. Milanfar, "Removing Atmospheric Turbulence via Space-Invariant Deconvolution," in *IEEE Transactions on Pattern Analysis and Machine Intelligence*, vol. 35, no. 1, pp. 157-170, Jan. 2013, doi: 10.1109/TPAMI.2012.82.

[12] K. K. Halder, M. Tahtali and S. G. Anavatti, "A new image restoration approach for imaging through the atmosphere," *IEEE International Symposium on Signal Processing and Information Technology*, Athens, Greece, 2013, pp. 000350-000355, doi:10.1109/ISSPIT.2013.6781906.

[13] R. C. Gonzalez and R. E. Woods, *Digital Image Processing*, Prentice Hall, 2018. ISBN: 978-0133356724.

[14] P. E. Robinson and Y. Roodt, "Blind deconvolution of Gaussian blurred images containing additive white Gaussian noise," *2013 IEEE International Conference on Industrial Technology (ICIT)*, Cape Town, South Africa, 2013, pp. 1092-1097, doi:10.1109/ICIT.2013.6505824.

[15] R. Mishra, N. Mittal and S. K. Khatri, "Digital Image Restoration using Image Filtering Techniques," *2019 International Conference on Automation, Computational and Technology Management (ICACTM)*, London, UK, 2019, pp. 268-272, doi:10.1109/ICACTM.2019.8776813.

[16] M. M. R. Khan, S. Sakib, R. B. Arif and M. A. B. Siddique, "Digital Image Restoration in Matlab: A Case Study on Inverse and Wiener Filtering," *2018 International Conference on Innovation in Engineering and Technology (ICIET)*, Dhaka, Bangladesh, 2018, pp. 1-6, doi:10.1109/CIET.2018.8660797.

[17] A. K. Jain, *Fundamentals of Digital Image Processing*, Prentice Hall, 1989. ISBN: 978-0133361650.

[18] A. Levin, Y. Weiss, F. Durand, and W. T. Freeman, "Understanding and evaluating blind deconvolution algorithms," *Proc. IEEE Conf. Computer Vision and Pattern Recognition*, 2009, doi:10.1109/CVPR.2009.5206861.

[19] L. Rudin, S. Osher, and E. Fatemi, "Nonlinear total variation-based noise removal algorithms," *Physica D: Nonlinear Phenomena*, vol. 60, no. 1-4, pp. 259-268, 1992, doi:10.1016/0167-2789(92)90242-F.

[20] B. R. Hunt, "The Application of Constrained Least Squares Estimation to Image Restoration by Digital Computer," in *IEEE Transactions on Computers*, vol. C-22, no. 9, pp. 805-812, Sept. 1973, doi:10.1109/TC.1973.5009169.

[21] M. Irani and S. Peleg, "Motion analysis for image enhancement: Resolution, occlusion, and transparency," *Journal of Visual Communication and Image Representation*, vol. 4, no. 4, pp. 324-335, 1993, doi:10.1006/jvci.1993.1032.

[22] W. H. Richardson, "Bayesian-Based Iterative Method of Image Restoration," *Journal of the Optical Society of America*, vol. 62, no. 1, pp. 55-59, 1972, doi:10.1364/JOSA.62.000055.

[23] L. B. Lucy, "An iterative technique for the rectification of observed distributions," *Astronomical Journal*, vol. 79, pp. 745, 1974, doi:10.1086/111605.

[24] S. Osher and J. A. Sethian, "Fronts propagating with curvature-dependent speed: Algorithms based on Hamilton-Jacobi formulations," *Journal of Computational Physics*, vol. 79, no. 1, pp. 12-49, 1988, doi:10.1016/0021-9991(88)90002-2.

[25] Nah, S., Kim, T. H., Lee, K. M. (2019). "REDS: A Dataset for Image and Video Restoration and Enhancement." *arXiv* preprint arXiv:1904.11490.

[26] M. Born and E. Wolf, *Principles of Optics*, Cambridge University Press, 1999. ISBN: 978-0521642224.

[27] F. Qin *et al*., "Blind Image Restoration with Horizontal Motion Blur Based on Point Spread Function Estimation in Frequency Domain," *2022 14th International Conference on Computer Research and Development (ICCRD)*, Shenzhen, China, 2022, pp. 286-290, doi:10.1109/ICCRD54409.2022.9730251.

[28] A. K. Soe and X. Zhang, "A simple PSF parameters estimation method for the de-blurring of linear motion blurred images using wiener filter in OpenCV," *2012 International Conference on Systems and Informatics (ICSAI2012)*, Yantai, China, 2012, pp. 1855-1860, doi:10.1109/ICSAI.2012.6223408.

[29] J. C. Russ, *The Image Processing Handbook*, 6th ed. Boca Raton, FL, USA: CRC Press, 2011. ISBN 9781138747494.

[30] Wei-Sheng Lai, Jian-Jiun Ding, Yen-Yu Lin and Yung-Yu Chuang, "Blur kernel estimation using normalized color-line priors," *2015 IEEE Conference on Computer Vision and Pattern Recognition (CVPR)*, Boston, MA, 2015, pp. 64-72, doi: 10.1109/CVPR.2015.7298601.

[31] Sunghyun Cho and Seungyong Lee, 2009, “Fast motion deblurring”, *ACM Trans. Graph.* 28, 5 (December 2009), 1–8. doi: 10.1145/1618452.1618491.

[32] J.S. Lim, *Two-Dimensional Signal and Image Processing*, Prentice Hall, 1990. ISBN 0139353224.

[33] J. P. Oliveira, M. A. T. Figueiredo and J. M. Bioucas-Dias, "Parametric Blur Estimation for Blind Restoration of Natural Images: Linear Motion and Out-of-Focus," in *IEEE Transactions on Image Processing*, vol. 23, no. 1, pp. 466-477, Jan. 2014, doi: 10.1109/TIP.2013.2286328.

[34] J. Huang and J. Jiang, "Motion parameters estimation based on improved radon transform for blurred star image," *2016 IEEE International Conference on Imaging Systems and Techniques (IST)*, Chania, Greece, 2016, pp. 42-47, doi: 10.1109/IST.2016.7738195.

[35] A. M. Deshpande and S. Patnaik, "Radon transform based uniform and non-uniform motion blur parameter estimation," *2012 International Conference on Communication, Information & Computing Technology (ICCICT)*, Mumbai, India, 2012, pp. 1-6, doi: 10.1109/ICCICT.2012.6398125.

[36] S. Mishra, R. S. Sengar, R. K. Puri and D. N. Badodkar, "Efficient motion blur parameters estimation under noisy conditions," *2014 IEEE International Conference on Computational Intelligence and Computing Research*, Coimbatore, India, 2014, pp. 1-5, doi: 10.1109/ICCIC.2014.7238308.

[37] M. J. Shah and U. D. Dalal, "Hough transform and cepstrum based estimation of spatial-invariant and variant motion blur parameters," *2014 International Conference on Advances in Electronics Computers and Communications*, Bangalore, India, 2014, pp. 1-6, doi: 10.1109/ICAECC.2014.7002425.

[38] M. J. Shah and U. D. Dalal, "Blind estimation of motion blur kernel parameters using Cepstral domain and Hough transform," *2014 International Conference on Advances in Computing*, Communications and Informatics (ICACCI), Delhi, India, 2014, pp. 992-997, doi: 10.1109/ICACCI.2014.6968241.

[39] Yan Ge, "Research on the blind restoration algorithm of motion-blurred image," *2016 IEEE Advanced Information Management*, Communicates, Electronic and Automation Control Conference (IMCEC), Xi'an, China, 2016, pp. 394-397, doi: 10.1109/IMCEC.2016.786724.

[40] C. -H. Chen, Z. Rui, K. -K. Tseng and J. -S. Pan, "Image Restoration for Linear Local Motion-Blur Based on Cepstrum," *2012 Sixth International Conference on Genetic and Evolutionary Computing*, Kitakyushu, Japan, 2012, pp. 332-335, doi: 10.1109/ICGEC.2012.102.

[41] A. M. Deshpande and S. Patnaik, "On improving accuracy of PSF estimation in spectral and cepstrum domain with morphological filtering," *2012 1st International Conference on Emerging Technology Trends in Electronics*, Communication & Networking, Surat, India, 2012, pp. 1-6, doi: 10.1109/ET2ECN.2012.6470092.

[42] Y. -j. Li and X. -g. Di, "Image mixed blur classification and parameter identification based on cepstrum peak detection," *2016 35th Chinese Control Conference (CCC)*, Chengdu, China, 2016, pp. 4809-4814, doi: 10.1109/ChiCC.2016.7554099.

[43] Y. -m. Liu and L. -f. Tian, "Approach to Optimizing Restoration of Motion Blur Images with Robust Blind Deconvolution Based on New Cepstrum and Total Variation," *2012 International Conference on Computer Science and Electronics Engineering*, Hangzhou, China, 2012, pp. 554-558, doi: 10.1109/ICCSEE.2012.174.

[44] Zhizhong Fu, Haiying Xian, Jin Xu and Xiaoqi Ge, "Evaluation of motion blur parameter based on cepstrum domain of the intentional restored image," *International Conference on Computational Problem-Solving*, Li Jiang, China, 2010, pp. 271-274.7.

[45] J. Han, C. Zhang, X. Shu and Z. Wang, "Joint Parameter Estimation of Mixed Blur for Image Restoration," *2023 8th International Conference on Signal and Image Processing (ICSIP)*, Wuxi, China, 2023, pp. 269-273, doi: 10.1109/ICSIP57908.2023.10271021.

[46] Q. -y. Wang, "Research on the motion-blurred direction by spectrum image analysis," *2014 9th IEEE Conference on Industrial Electronics and Applications*, Hangzhou, China, 2014, pp. 1125-1129, doi: 10.1109/ICIEA.2014.6931334.

[47] X. Kang, Q. Peng, G. Thomas and C. Yu, "Blind Image Restoration using the Cepstrum Method," *2006 Canadian Conference on Electrical and Computer Engineering*, Ottawa, ON, Canada, 2006, pp. 1952-1955, doi: 10.1109/CCECE.2006.277481.

[48] X. Kang, Q. Peng, G. Thomas and C. Yu, "Blind Image Restoration using the Cepstrum Method," *2006 Canadian Conference on Electrical and Computer Engineering*, Ottawa, ON, Canada, 2006, pp. 1952-1955, doi: 10.1109/CCECE.2006.277481.

[49] Bracewell, R. N. (2000)., *The Fourier Transform and Its Applications*, (3rd Edition). McGraw-Hill, ISBN-10: 0073039381.

[50] Andrews, H. C., & Hunt, B. R. (1977), *Digital Image Restoration*, Prentice Hall, ISBN-10: 0132142139.

[51] Rudin, L. I., Osher, S., & Fatemi, E. (1992), "Nonlinear total variation-based noise removal algorithms," *Physica D: Nonlinear Phenomena*, 60(1-4), 259-268, doi: 10.1016/0167-2789(92)90242-F.

[52] Chan, T. F., & Shen, J., (2005), "Image Processing and Analysis: Variational, PDE, Wavelet, and Stochastic Methods," *Society for Industrial and Applied Mathematics (SIAM)*, ISBN-10: 089871589X.

[53] Osher, S., Burger, M., Goldfarb, D., Xu, J., & Yin, W. (2005), "An iterative regularization method for total variation-based image restoration," *Multiscale Modeling & Simulation*, 4(2), 460-489, doi:10.1137/040605412.

[54] Bishop, C. M. (2006), *Pattern Recognition and Machine Learning*, Springer, ISBN978-0-387-31073-2.

[55] Friedman, J., Hastie, T., & Tibshirani, R. (2001), *The Elements of Statistical Learning*. Springer, eBook ISBN978-0-387-84858-7.

[56] Fish, D. A., Brinicombe, A. M., Pike, E. R., & Walker, J. G. (1995), "Blind deconvolution by means of the Richardson–Lucy algorithm," *Journal of the Optical Society of America A*, 12(1), 58-65, doi: 10.1364/JOSAA.12.000058.

[57] Snyder, D. L., Hammoud, A. M., & White, R. L. (1993), “Image recovery from data acquired with a charge-coupled-device camera,” *Journal of the Optical Society of America A*, 10(5), 1014-1023, doi: 10.1364/JOSAA.10.001014.

[58] Shewchuk, Jonathan Richard. “An Introduction to the Conjugate Gradient Method Without the Agonizing Pain,” *Technical Report*, Carnegie Mellon University, USA. 1994.

[59] D. Kundur and D. Hatzinakos, "Blind image deconvolution," in *IEEE Signal Processing Magazine*, vol. 13, no. 3, pp. 43-64, May 1996, doi: 10.1109/79.489268.

[60] Bilmes, J. A. “A Gentle Tutorial of the EM Algorithm and its Application to Parameter Estimation for Gaussian Mixture and Hidden Markov Models”, *International Computer Science Institute*, 1998.

[61] V.-I. Ungureanu, P. Negirla, and A. Korodi, “Image-Compression Techniques: Classical and ‘Region-of-Interest-Based’ Approaches Presented in Recent Papers,” *Sensors*, vol. 24, no. 3, Art. no. 3, Jan. 2024, doi: 10.3390/s24030791.

[62] D. Zhan, X. Zeng, W. Li, Y. Liu and Z. Xiong, "Blur kernel estimation using normal sinh-arcsinh model based on simple lens system," *2017 IEEE 19th International Workshop on Multimedia Signal Processing (MMSP)*, Luton, UK, 2017, pp. 1-6, doi: 10.1109/MMSP.2017.8122293.

[63] F. Šroubek, T. Kerepecký and J. Kamenický, "Iterative Wiener Filtering for Deconvolution with Ringing Artifact Suppression," 2019, *27th European Signal Processing Conference (EUSIPCO)*, A Coruna, Spain, 2019, pp. 1-5, doi: 10.23919/EUSIPCO.2019.8903114.

[64] Jingyun Liang, Jiezhang Cao, Yuchen Fan, Kai Zhang, Rakesh Ranjan, Yawei Li, Radu Timofte, Luc Van Gool, " VRT: A Video Restoration Transformer", *ArXiv*, 2022, doi: doi.org/10.48550/arXiv.2201.12288.

[65] Xintao Wang, Kelvin C.K. Chan, Ke Yu, Chao Dong, Chen Change Loy, "EDVR: Video Restoration with Enhanced Deformable Convolutional Networks", *ArXiv*, 2019, doi: doi.org/10.48550/arXiv.1905.02716.

[66] “Deblurring on REDS”, paperswithcode.com/sota/deblurring-on-reds

[67] Ahlad Kumar, “Deblurring of motion blurred images using histogram of oriented gradients and geometric moments”, *Signal Processing: Image Communication*, 2017, doi: doi.org/10.1016/j.image.2017.03.016.